Finite-cluster typical medium theory for disordered electronic systems

C. E. Ekuma, C. Moore, H. Terletska, K.-M. Tam, J. Moreno, M. Jarrell, and N. S. Vidhyadhiraja

Phys. Rev. B **92**, 014209 — Published 24 July 2015

DOI: 10.1103/PhysRevB.92.014209

Finite Cluster Typical Medium Theory for Disordered Electronic Systems

C. E. Ekuma,* C. Moore, H. Terletska, K.-M. Tam, J. Moreno, and M. Jarrell†
Department of Physics & Astronomy, Louisiana State University, Baton Rouge, Louisiana 70803, USA and Center for Computation & Technology, Louisiana State University, Baton Rouge, Louisiana 70803, USA

N. S. Vidhyadhiraja
Theoretical Sciences Unit, Jawaharlal Nehru Center for Advanced Scientific Research, Bangalore, 560064, India

We use the recently developed typical medium dynamical cluster (TMDCA) approach [Ekuma *et al.*, *Phys. Rev. B* ***89****, 081107 (2014)*] to perform a detailed study of the Anderson localization transition in three dimensions for the Box, Gaussian, Lorentzian, and Binary disorder distributions, and benchmark them with exact numerical results. Utilizing the non-local hybridization function and the momentum resolved typical spectra to characterize the localization transition in three dimensions, we demonstrate the importance of both spatial correlations and a typical environment for the proper characterization of the localization transition in all the disorder distributions studied. As a function of increasing cluster size, the TMDCA systematically recovers the re-entrance behavior of the mobility edge for disorder distributions with finite variance, obtaining the correct critical disorder strengths, and shows that the order parameter critical exponent for the Anderson localization transition is universal. The TMDCA is computationally efficient, requiring only a small cluster to obtain qualitative and quantitative data in good agreement with numerical exact results at a fraction of the computational cost. Our results demonstrate that the TMDCA provides a consistent and systematic description of the Anderson localization transition.

PACS numbers: 72.15.Rn, 72.20.Ee, 71.23.An, 71.30.+h,64.70.Tg

I. INTRODUCTION

Disorder is ubiquitous in materials and can drastically alter their properties, in particular, their electronic structure and transport properties, and even may induce electron localization. This phenomenon is known as the Anderson metal-insulator-transition.[1–5] Here, the transition from a metal to an insulator is not characterized by the vanishing of the charge carrier density but by the cancellation of the hybridization paths accompanying the quantum localization of the wave functions due to coherent backscattering from random impurities, deep-trapped states, etc. As a result, electrons that occupy such exponentially localized states are restricted to finite regions of space, and hence cannot contribute to transport. The Anderson insulator is gapless indicating that the single-particle excitations are essential in determining its physical properties especially at low energies. While there has been significant progress in the quest to understand this phenomenon, a proper effective mean-field treatment is not yet fully developed.

There have been numerous theoretical studies of disordered electron systems employing computational techniques of varying complexity not limited to numerically exact methods including exact diagonalization, transfer matrix, and kernel polynomial methods,[4,6–15] various renormalization group techniques,[16–18] and mean field theories.[19–25] While numerical exact methods have been successfully used to study Anderson localization, they generally require the treatment of large clusters and the use of powerful computers. As a result, they are difficult to extend to the treatment of interacting systems or chemically specific models. An alternative approach is offered by mean-field theories such as the coherent potential approximation and its extensions.[23,24,26] They map the lattice onto relatively small self-consistently embedded clusters. These methods have been successfully extended to the treatment of interacting disordered systems and to chemically realistic models. Unfortunately, these methods have been woeful in the treatment of Anderson localization due mainly to the averaging procedure utilized and improvements in the environment describing the effective medium have been limited to single sites.

Due to the central role a mean-field theory that properly describes the Anderson localization transition (ALT) may play for further progress in the study of electron localization, there is a need to formulate such theory. Furthermore, a well-known long historical dichotomy exists between the mean-field results and the numerical data for the Anderson localization transition. Here, we demonstrate that the dichotomy can be reconciled by incorporating spatial fluctuations in a typical environment into the mean-field theory thereby offering a solution to this long-standing problem and providing a systematic framework in the mean-field theory of Anderson localization.

The most commonly used self-consistent mean-field theory, in the study of disordered electron systems, is the coherent potential approximation (CPA).[23,24] In the CPA, the original disordered lattice is replaced by an impurity placed in an averaged local (momentum-independent) effective medium. While the CPA successfully describes some one-particle properties, such as the density of states (DOS) in substitutional disordered alloys,[23,27] it fails to describe the Anderson localization transition. This failure stems, in part, from the single site nature of the CPA, as it is unable to capture cru-

cial multiple backscattering interference effects that lead to electron localization. Cluster extensions of the CPA, like the dynamical cluster approximation (DCA)[26,28,29] and molecular CPA[30], allow for the incorporation of such non-local spatial correlations; however, they still fail to describe the Anderson localization transition. The arithmetic averages of random one-particle quantities (e.g., density of states) calculated within such mean-field theories cannot distinguish between extended and localized states and are not critical at the Anderson transition.[1,31–33] Hence, such average quantities cannot be used as an order parameter. This is the reason that most mean-field theories like the CPA[34] and its cluster extensions including the DCA,[28,29,35] fail to provide a proper description of Anderson localization in disordered systems. This failure is intrinsic to these theories as the algebraically averaged quantities, i.e., the averaged density of states, always favor the metallic state. This can be understood from the fact that in an infinite system of localized states, the average density of states is nothing but the global density of states, which is a smooth function of the disorder strength near the critical point while the local density of states becomes discrete with a non-trivial system size dependence (see e.g., Refs.25, 31, 32, 36–40 for a detailed discussion). Further, due to the large fluctuations in the local Green function, its *typical value* is far removed from the average one[41] as such, the local average Green function, which characterizes these mean-field environments, does not have any information about the *typical nature* of the local order parameter needed to signal a phase transition. In Subsection III 1, we will demonstrate the failures of finite cluster extensions of the CPA in characterizing the Anderson localization transition using the DCA.

Finding a proper single-particle order parameter for the Anderson localization transition capable of distinguishing between the localized and extended states is a major challenge in the study of disordered electronic systems. In contrast to the arithmetic average, the geometrical average[25,37,39,42,43] gives a better approximation to the most probable value of the local density of states. Dobrosavljević *et al.*[25] developed the typical medium theory (TMT) to study disordered systems, where the typical density of states (TDOS), approximated using the geometrical averaging over disorder configurations, is used instead of the arithmetically averaged local density of states. They demonstrated that the TDOS vanishes continuously as the strength of the disorder increases towards the critical point and it can be used as an effective mean-field order parameter for the Anderson localization transition.

While the single-site TMT has been shown to be successful in describing localized electron states, it still has several drawbacks. In particular, it does not provide a proper description of the critical behavior of the Anderson localization transition in three dimensions (3D). As a local approximation, the TMT neglects the effects of coherent backscattering and, as a result, the critical disorder strength obtained is $W_c^{TMT} = 1.65$ instead of the numerically exact value $W_c \approx 2.1$[5,10,44–49] for the box distribution (in our units). Also, the *universal* order parameter critical exponent (which has also been called the *typical order parameter exponent*)[42] β obtained in the local TMT is $\beta^{TMT} \approx 1.0$ whereas its recently reported value is $\beta \approx 1.67$.[46,50] Another crucial drawback of the single site TMT in 3D is its inability to capture the reentrance behavior of the mobility edge (energy separating extended and localized electron states) demonstrated in exact numerical studies[47,51,52] for the disorder distributions with finite variance: the box and Gaussian disorder distributions. The TMT also underestimates the extended state regions in all the disorder distributions studied in this paper.

The inadequacies of the single-site TMT can be remedied by incorporating spatial (non-local) correlations by constructing its cluster extension. This can be achieved by using the DCA or molecular CPA schemes, which systematically incorporate the missing non-local effects.

In this paper, we show in detail a successful extension of the local TMT to its cluster version using ideas from the DCA. We demonstrate how the finite cluster extension of the local TMT is able to systematically solve all the crucial drawbacks of the single-site TMT, indicating the necessity to include the missing non-local effects. One of the features of the Anderson localization transition in three dimensions is the non-self-averaging nature of the local quantities close to the localization transition which obtain a highly skewed (log-normal) distribution. Hence, special care must be taken in constructing a cluster extension of the TMT. To avoid such self-averaging issues in the TDOS, we developed the typical medium dynamical cluster approximation (TMDCA),[1] which properly characterizes the Anderson localization transition in 3D and does not suffer from the self-averaging, by explicitly separating the local part of the TDOS and treating it with a geometric average over disorder configurations. Hence, we are able to obtain a proper TDOS that characterizes the Anderson localization in 3D. We demonstrate the versatility of our method by applying it to the box, Gaussian, Lorentzian, and binary disorder distributions and benchmark it with numerically exact methods.

The typical medium dynamical cluster approximation scheme is demonstrated to be a systematic, self-consistent effective medium theory for characterizing electron localization. As a function of increasing cluster size, we demonstrate that the TMDCA achieves convergence of both the critical disorder strength and the trajectories of the mobility edge as a function of cluster size. Furthermore, the TMDCA fulfills all the essential requirements expected of a "successful" cluster theory.[28,53] We find that the TMDCA scheme is a systematic self-consistent effective medium theory to study Anderson localization transition in three-dimensions, which i) recovers the original single-site TMT scheme at cluster size $N_c = 1$; ii) recovers the DCA results at small disorder strength (when most states are metallic); iii) pro-

vides a proper way to separate the energy scales such that the characteristic mobility edge behavior (for the disorder distributions with finite variance) is recovered; iv) captures the critical behavior of the Anderson localization transition with correct critical disorder strength W_c and order parameter critical exponent β, and provides the correct description of the Anderson insulator at large disorder strength (when all states are localized); and v) fulfills all the essential requirements expected of a "successful" cluster theory.[28,53]

The main problem addressed in this paper is how the mobility edge energies vary with disorder strength, their trajectories, and what happens to these trajectories in the proximity of the Anderson localization transition. Furthermore, since the DCA always becomes exact when $N_c \to \infty$, the main role of the effective medium in approaches based on the DCA, or its extensions, is to accelerate this convergence. For the ALT, we find that the effective medium formed from the average Green function does not converge as N_c becomes large, rather it is only able to describe the precursors to localization (cf. Section III 1). However, we find that a number of effective media based upon the geometrically averaged density of states provide convergent results, i.e., order parameter. So far, we find that the fastest convergence is provided by the TMDCA.

The rest of this paper is organized as follows: following the introduction in this Section I, we present the model and describe the details of the formalism in Section II. We present the results of our calculations in Section III. The absence of localization in the DCA (shows only precursor to localization) is described in III 1. Detailed analysis of how we avoid self-averaging as the size of the cluster is increased is discussed in III 2. Then in III 3, we describe how to treat the states close to criticality where the hybridization function vanishes leading to the development of poles (delta functions) in the imaginary part of the cluster-excluded Green function, $\mathcal{G}(K,\omega)$. A detailed analysis of our results for the box disorder distribution is presented in Subsection III A. Subsection III B presents our results for the binary disorder distribution. In Subsection III C, we present our results for the Gaussian disorder distribution while Subsection III D shows the results of our computations for the Lorentzian distribution. In Subsection III E, we discuss in detail the procedure for obtaining the critical parameters especially the order parameter critical exponent β for the various disorder distributions, while in Subsection III F, we address the discrepancy observed in the trajectories of the mobility edge energies at higher disorder strength. We summarize and discuss future directions in Section IV. In appendices A and B, we present a concise description of the developed transfer matrix and kernel polynomial methods, respectively, used in benchmarking the TMDCA.

II. METHOD

We consider the Anderson model of non-interacting electrons subjected to a random potential. The Hamiltonian (for spinless fermions) is given by

$$H = -\sum_{<ij>} t_{ij}(c_i^\dagger c_j + h.c.) + \sum_i (V_i - \mu) n_i. \quad (1)$$

The first term is the kinetic energy operator due to hopping of electrons on a lattice. The operators $c_i^\dagger(c_i)$ create (annihilate) a quasiparticle on site i, and t_{ij} is the hopping matrix element between nearest-neighbor $\langle i,j\rangle$. The second term is the disordered part parameterized by a local potential V_i, which is a random quantity distributed according to some specified probability distribution $P(V_i)$, $n_i = c_i^\dagger c_i$ is the number operator, and μ is the chemical potential. We set $4t = 1$ as the energy unit. In our analysis, we use different disorder distributions. In particular, we consider the box (Bo), Gaussian (Ga), Lorentzian (Lo), and binary (Bi) distributions, respectively, with the corresponding distribution functions $P(V_i)$

$$P_{Bo}(V_i) = \frac{1}{2W_{Bo}}\Theta(W_{Bo} - |V_i|), \quad (2a)$$

$$P_{Ga}(V_i) = \sqrt{\frac{3}{2\pi W_{Ga}^2}} e^{-3V_i^2/(2W_{Ga}^2)}, \quad (2b)$$

$$P_{Lo}(V_i) = \frac{W_{Lo}}{\pi(V_i^2 + W_{Lo}^2)}, \quad (2c)$$

$$P_{Bi}(V_i) = c_a\delta(V_i - W_A) + c_b\delta(V_i - W_B), \quad (2d)$$

where $\Theta(x)$ is the step function, c_a is the concentration of the host A atom, $c_b = 1 - c_a$ is the concentration of the impurity B atom, and the strength of the disorder in units of $4t$ is parameterized by W (W_A and W_B for the binary alloy model). We have scaled W_{Ga} such that the second moments of the P_{Bo} and P_{Ga} agree with each other (i.e., we set the variance of the Gaussian distribution equal to that of the box distribution: $\sigma^2 = W^2/3$) in the event that W_{Bo}=W_{Ga} to enable comparison. Since the Lorentzian distribution lacks a second moment, the disorder values cannot be directly compared with that of either the box or Gaussian distributions. We introduce a short-hand notation for disorder averaging $\langle ...\rangle = \int dV_i P(V_i)(...)$.

To solve the Hamiltonian (1) different methods will be used including the DCA,[28] the cluster typical medium theory,[33] and the recently developed typical medium dynamical cluster approximation (TMDCA).[1] We will compare these results to those obtained from numerical methods like the kernel polynomial method (KPM)[9,12–14] and the transfer matrix method (TMM).[4,10–14]

The TMDCA utilizes the self-consistent framework of the standard dynamical cluster approximation[28] with the important usage of an environment defined by a typical non-local hybridization function. In particular, the

TMDCA maps the given disordered lattice system onto a finite cluster which is embedded in an effective self-consistent typical medium. Note that unlike the usual DCA scheme, where the effective medium is constructed via algebraic averaging over disorder configurations, the TMDCA scheme uses geometric averaging. By mapping a d-dimensional lattice to a finite small cluster containing $N_c = L_c^d$ sites, where L_c is the linear dimension of the cluster, we dramatically reduce the computation effort.[35] Unlike the single-site methods commonly used to study disordered systems, such as the coherent potential approximation (CPA)[23,34] or the local TMT,[25] the TMDCA ensures that non-local spatial fluctuations, neglected in single-site approaches, are systematically incorporated as the cluster size N_c increases. Short length scale correlations are treated exactly inside the cluster, while the long length scale correlations are treated within the typical medium.

Algorithm: The details of the TMDCA formalism are described below. The non-local (**K**-dependent) disorder average cluster density of states is given as

$$\rho^c_{avg}(\mathbf{K},\omega) = \langle \rho^c(\mathbf{K},\omega,V)\rangle = -\frac{1}{\pi}\langle \Im G^c(\mathbf{K},\mathbf{K},\omega,V)\rangle, \tag{3}$$

where the superscript 'c' denotes cluster and $\langle ...\rangle$ is the disorder average. For a single site $N_c = 1$, we recover the CPA. The **K**-dependent cluster Green function is obtained from the site dependent Green function $G_c(i,j,\omega)$ via the Fourier transform:

$$G^c(\mathbf{K},\mathbf{K},\omega) = \frac{1}{N_c}\sum_{i,j} e^{i\mathbf{K}\cdot(\mathbf{R}_i-\mathbf{R}_j)} G_c(i,j,\omega). \tag{4}$$

Within the TMDCA, for each cluster configuration, we first obtain $\rho^c(\mathbf{K},\omega) = -\Im G^c(\mathbf{K},\mathbf{K},\omega)/\pi$. It can be shown via the Lehmann representation,[54,55] that $\rho^c(\mathbf{K},\omega) \geq 0$ for each **K**, ω, and disorder configuration.

As mentioned above, in the TMDCA, the local part of the cluster-momentum-resolved typical density of states is separated and treated with geometrical averaging over the disorder configurations, to avoid self-averaging as the cluster size increases. The obtained cluster typical spectra are given by

$$\rho^c_{typ}(\mathbf{K},\omega) = \overbrace{\exp\left(\frac{1}{N_c}\sum_{i=1}^{N_c}\langle \ln \rho^c_i(\omega,V)\rangle\right)}^{\text{local TDOS}} \times \underbrace{\left\langle \frac{\rho^c(\mathbf{K},\omega,V)}{\frac{1}{N_c}\sum_i \rho^c_i(\omega,V)}\right\rangle}_{\text{non-local}}. \tag{5}$$

From Eq. 5, the disorder averaged typical cluster Green function is obtained using the Hilbert transform

$$G^c_{typ}(\mathbf{K},\omega) = \int d\omega' \frac{\rho^c_{typ}(\mathbf{K},\omega')}{\omega-\omega'}. \tag{6}$$

A schematic TMDCA self-consistency is shown in Fig. 1.

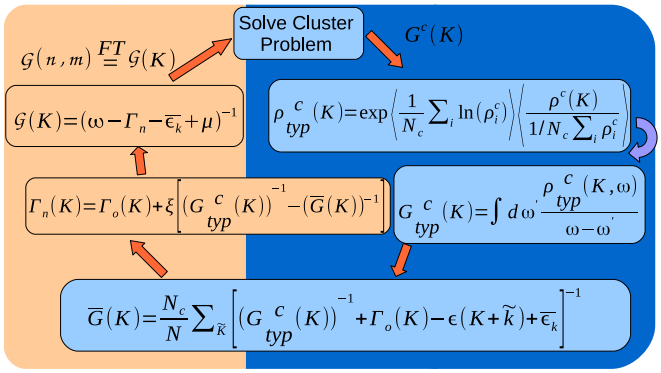

FIG. 1. (Color online) The self-consistent loop of the TMDCA.

The TMDCA iterative procedure is outlined below.

1. The TMDCA iterative procedure begins by proposing an initial guess for the hybridization function $\Gamma_o(\mathbf{K},\omega)$, where the subscript '$o$' denotes old. The choice of the starting guess for the hybridization function may be based on a priori knowledge, i.e., having information about the self-energy $\Sigma(\mathbf{K},\omega)$ and cluster Green function $G^c(\mathbf{K},\omega)$, $\Gamma_o(\mathbf{K},\omega)$ can be calculated as

$$\Gamma_o(\mathbf{K},\omega) = \omega - \overline{\epsilon}(\mathbf{K}) + \mu - \Sigma(\mathbf{K},\omega) - 1/G^c(\mathbf{K},\omega) \tag{7}$$

where $\overline{\epsilon}(\mathbf{K}) = N_c/N\sum_{\tilde{k}}\epsilon(\mathbf{K}+\tilde{k})$ is the coarse-grained bare dispersion with $\tilde{k}$ summed over N/N_c momenta inside the cell centered at the cluster momentum **K**.[29] However, if nothing is known a priori, $\Gamma_o(\mathbf{K},\omega)$ set to a small imaginary number may serve as the starting point.

2. After setting up the cluster problem, we calculate the cluster-excluded Green function $\mathcal{G}(\mathbf{K},\omega)$ as

$$\mathcal{G}(\mathbf{K},\omega) = (\omega - \Gamma_o(\mathbf{K},\omega) - \overline{\epsilon}(\mathbf{K}) + \mu)^{-1}. \tag{8}$$

Since the cluster problem is solved in real space, we then Fourier transform $\mathcal{G}(\mathbf{K},\omega)$: $\mathcal{G}_{n,m} = \sum_{\mathbf{K}} \mathcal{G}(\mathbf{K}) \exp(i\mathbf{K}\cdot(r_n - r_m))$.

3. Next, to solve the cluster problem, we stochastically generate random configurations of the disorder potential V, and calculate the corresponding cluster Green function as

$$G^c(V) = (\mathcal{G}^{-1} - V)^{-1}. \quad (9)$$

This is Fourier transformed to $G^c(\mathbf{K},\mathbf{K},\omega)$ to obtain the cluster density of states $\rho^c(\mathbf{K},\omega) = -\frac{1}{\pi}\Im G^c(\mathbf{K},\mathbf{K},\omega)$. The typical cluster spectra is then calculated via geometric averaging using Eq. 5. Then, we calculate the disorder averaged, typical cluster Green function $G^c_{typ}(\mathbf{K},\omega)$ via the Hilbert transform using Eq. 6. We note the advantage of the stochastic sampling of the disorder configurations. Here, each of the disorder configurations is statistically independent of the others. Thus, for example, for the binary disorder distribution, instead of enumerating all configurations, which scales as 2^{Nc}, we do a stochastic sampling of the disorder configurations. This greatly reduces the computational cost, at the expense of a small sampling error, enabling us to study larger clusters. We also enforce all of the cluster translational and point group symmetries, effectively generating more configurations. With this, the number of disorder realizations needed to obtain a converged solution falls with increasing cluster size. For a typical 64 site cluster, with box disorder, about 500 disorder realizations are enough to produce high-quality data. The code scales like $A(N_c)N_c^3$ due to the matrix inversion in Eq. 9, but the prefactor $A(N_c)$, also depends on N_c since fewer self-consistency iterations and disorder configurations are needed for larger clusters. Hence, $A(N_c)$ falls with increasing cluster size.

4. After solving the cluster problem, we use the typical cluster Green function, $G^c_{typ}(\mathbf{K},\omega)$, to calculate the coarse-grained cluster Green function of the lattice $\overline{G}(\mathbf{K},\omega)$ as

$$\overline{G}(\mathbf{K},\omega) = \int \frac{N_0^c(\mathbf{K},\epsilon)d\epsilon}{(G^c_{typ}(\mathbf{K},\omega))^{-1} + \Gamma(\mathbf{K},\omega) - \epsilon + \overline{\epsilon}(\mathbf{K})}, \quad (10)$$

where $N_0^c(\mathbf{K},\epsilon)$ is the bare partial density of states.

5. We then close our self-consistency loop by updating the new hybridization function using linear mixing

$$\Gamma_n(\mathbf{K},\omega) = \Gamma_o(\mathbf{K},\omega) + \xi[(G^c_{typ}(\mathbf{K},\omega))^{-1} - (\overline{G}(\mathbf{K},\omega))^{-1}] \quad (11)$$

where the subscripts 'n' and 'o' denote new and old, respectively. The mixing parameter $\xi > 0$ controls the ratio of the new and old $\Gamma(\mathbf{K},\omega)$ entering the next iteration. For very small ξ, convergence may be slowed down unnecessarily, while for very large ξ, oscillations about the self-consistent solution may occur. Instead of linear mixing, the convergence of the computations can be improved by using the Broyden method.[56]

6. We repeat the above procedure until the hybridization function converges to the desired accuracy, $\Gamma_o(\mathbf{K},\omega) = \Gamma_n(\mathbf{K},\omega)$. When this happens, the Green functions are also converged, $\overline{G}(\mathbf{K},\omega) = G^c_{typ}(\mathbf{K},\omega)$ within the computational error.

We note that our formalism preserves causality just as the DCA,[28] since all the Green functions are causal, both the average density of states (ADOS) and the TDOS calculated from them are positive definite. Also, we observe that as N_c increases, our method systematically interpolates between the local TMT and the exact result.

For reproducibility, we specify in Table I the cluster geometries and other important parameters of the clusters used in our computations. The parameters of Table I include the lattice vectors $(\vec{a}_1, \vec{a}_2, \vec{a}_3)$, and the cubicity (C).[57] The cubicity is given as $C = \max(c_1, c_1^{-1}) \times \max(c_2, c_2^{-1})$, where $c_1 = 3^{1/2}l/d$ and $c_2 = 2^{1/2}l/f$ are cluster parameters defined by the geometric mean of the lengths of the four body diagonals of the cluster, $d = (d_1 d_2 d_3 d_4)^{1/4}$, the six-face diagonals, $f = (f_1 f_2 f_3 f_4 f_5 f_6)^{1/6}$, and the edges, $l = (l_1 l_2 l_3)^{1/3}$.[57] $C = 1$ is for a perfect cube, and $C > 1$ otherwise. Following this criterion, clusters $N_c = 1$, 64, 125, and 216 are perfect cubes.

TABLE I. Three-dimensional (3D) cluster geometries utilized in our calculations. The a_i denote the cluster lattice vectors and C is the cubicity.

N_c	$\vec{a}_1$	$\vec{a}_2$	$\vec{a}_3$	C
1	(1, 0, 0)	(0, 1, 0)	(0, 0, 1)	1.000
38	(1, 2, 3)	(3, -1, -2)	(2, -2, 2)	1.087
64	(4, 0, 0)	(0, 4, 0)	(0, 0, 4)	1.000
125	(5, 0, 0)	(0, 5, 0)	(0, 0, 5)	1.000
216	(6, 0, 0)	(0, 6, 0)	(0, 0, 6)	1.000

III. RESULTS AND DISCUSSION

Before presenting our main results in detail, we will first review the characteristics of the DCA. Despite its advantage over the CPA, it shares the same behavior with the CPA in that it is unable to detect the localization transition in a disordered electron system.[26] We will also elaborate on the details of how self-averaging is avoided in the TMDCA as the cluster size is increased. This becomes imperative since in the cluster, self-averaging

will ultimately destroy our ability to detect the Anderson localization transition. Both the inability of the DCA to capture the Anderson localization transition and how self-averaging is avoided in the TMDCA will be demonstrated using the box disorder distribution.

1. *Absence of Localization in the DCA*

The dynamical cluster approximation (DCA) unlike the coherent potential approximation (CPA) incorporates non-local spatial correlations systematically as the size of the cluster is increased. While spatial correlations are an important ingredient in the localization transition in disordered electron systems, the DCA effective medium is characterized by arithmetic averaging over the disorder configurations. As explained above and will be demonstrated below, even a typically defined medium without a proper treatment of the typical density of states (the local part of the typical density of states needs to be separated and treated explicitly using geometrical averaging), reduces to the DCA for large clusters. In Fig. 2 (left panel), we show the ADOS at small and large disorder strengths for the single-site ($N_c = 1$) and finite cluster ($N_c = 64$) calculations. We also show in Fig. 2 (right panel) the probability $P(t) = \langle |G(l,l,t)|^2 \rangle$ of an electron remaining at a site l at long time t calculated within the single-site and finite cluster DCA[26] scheme while the insets depict the probability of an electron remaining on a site l for all time: $P(t \to \infty, \eta) = \lim_{t\to\infty} \langle |G(l,l,t)|^2 \rangle = = \lim_{\eta\to 0} \frac{\eta}{\pi} \int_{-\infty}^{\infty} d\epsilon \langle |G(l,l,\epsilon + i\eta)|^2 \rangle$.

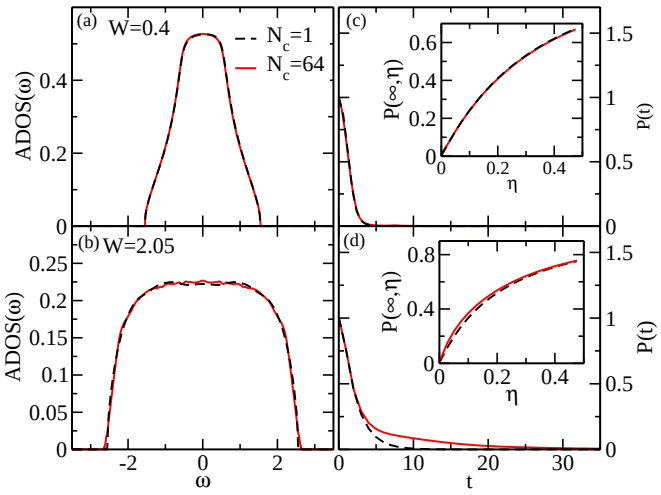

FIG. 2. (Color online). Left panels: The average density of states calculated using the DCA for small and large disorder strengths[26]. Right panels: The probability of an electron remaining on a site after time t, $P(t) = \langle |G(l,l,t)|^2 \rangle$. The insets in the plots on the right are the probability of an electron remaining on a site for all time $P(t \to \infty, \eta) = \lim_{t\to\infty} \langle |G(l,l,t)|^2 \rangle = = \lim_{\eta\to 0} \frac{\eta}{\pi} \int_{-\infty}^{\infty} d\epsilon \langle |G(l,l,\epsilon + i\eta)|^2 \rangle$ for the $N_c = 1$ (black) and 64 (red), respectively. The ADOS is not critical at the Anderson transition. The non-critical behavior in the DCA can also be inferred from P(t), which decays rather fast instead of remaining constant, and $P(t,\eta)$ that extrapolates to zero instead of to a finite value when many of the states are localized. The DCA only shows a precursor to Anderson localization as manifested in P(t) for large disorder strength for the finite cluster sizes.

$P(\infty,\eta)$ is expected [26] to be nonzero for any fraction of the localized states in the spectrum of the eigenstates of the disordered system.[28,53,58,59] As is evident from the inset of the right panel of Fig. 2, the plot of $P(\infty,\eta)$ versus η, $P(\infty,\eta)$ extrapolates to zero even very close to the critical disorder strength for both $N_c = 1$ and 64, respectively.

Also observe from Fig. 2 (left panel), the ADOS is not critical at the Anderson transition. This is manifested in the $P(t)$ plot since for a localized state, $P(t)$ is expected to be finite. For $N_c = 1$, $P(t)$ falls quickly with time regardless of the disorder strength. However, for $N_c = 64$, the electrons remain localized for longer times as the disorder strength is increased. This can be understood by noting that each site on the cluster is coupled to a non-interacting translationally invariant host into which electrons can escape. Hence, if a finite density of states exists at some energy, the corresponding states are guaranteed to be extended unless the hybridization rate between the host and the cluster vanishes. Indeed, this is the case in the DCA. The imaginary part of the integrated hybridization (escape) rate $(-\Im \int \Gamma(\mathbf{K},\omega) d\mathbf{K} d\omega)$ between the cluster and the host as a function of disorder strength (W) remains constant regardless of the strength of the disorder (cf. insets of Figs. 6, 14 and 16, for different disorder distributions). It does not go to zero as needed for a localization transition in the typical medium context. Thus, the DCA is only able to capture the precursor to Anderson localization as the cluster size, but not the disorder strength increases.

2. *Avoiding Self-averaging*

The averaging procedure used to calculate the typical spectra is not unique. As noted above, our initial attempt to formulate a cluster version of the TMT reproduced the expected behavior in one and two dimensions as N_c is increased.[33] However, in three dimensions, applying the algorithm directly will lead to an effective self-averaging for large clusters. This is due to the fact that close to criticality, there exist distinct localized and extended states above and below the localization edge given by the TDOS with an energy scale difference that can span an order of magnitude. These energy scales need to be treated differently. This can be seen by investigating the spectra where the local part of the TDOS is not explicitly separated and treated with a geometric

averaging over disorder realizations:

$$\rho^c_{typ}(\mathbf{K},\omega) = \exp\langle \ln \rho^c(\mathbf{K},\omega,V_i)\rangle\,. \tag{12}$$

In forming the Fourier transform

$$\rho^c(\mathbf{K},\omega,V_i) = -\frac{1}{\pi}\Im\left[\frac{1}{N_c}\sum_{X,X'} e^{i\mathbf{K}\cdot(X-X')}G^c(X,X',\omega,V_i)\right] \tag{13}$$

we average over the cluster coordinates X and X', including the local part, $X = X'$. So, the local DOS is first averaged over the cluster sites and then Fourier transformed making the local part of $\rho^c(\mathbf{K},\omega)$. Hence for large clusters, this reduces to linear averaging of the local part instead of geometrical averaging. As a consequence, the host Green function constructed from $\rho^c_{typ}(\mathbf{K},\omega)$ of Eq. 12 is unaware of the TDOS and thus, it is unable to distinguish between the energies above and below the localization edge. To avoid such self-averaging in the TDOS, we proposed the Typical Medium DCA (TMDCA) method.[1] Here, the cluster-momentum-resolved typical density of states (TDOS) for each $\mathbf{K}$ is split into local and non-local parts. The local part is treated with geometrical averaging over disorder configurations, while the non-local part is treated with an algebraic or geometric averaging over the disorder configuration.

To do this, we have utilized two schemes. The first scheme is what we call *linear-log* procedure, which is used in this study. Here, we treat the local part with a geometrical averaging while the non-local part is approximated algebraically using linear averaging as

$$\rho^c_{typ}(\mathbf{K},\omega) = \exp\left(\frac{1}{N_c}\sum_{i=1}^{N_c}\langle\ln\rho^c_i(\omega,V_i)\rangle\right)\times \left\langle\frac{\rho^c(\mathbf{K},\omega,V_i)}{\frac{1}{N_c}\sum_i\rho^c_i(\omega,V_i)}\right\rangle. \tag{14}$$

The second scheme is what we call the *log-log* procedure, which again involves the treatment of the local part with geometrical averaging; however, the non-local part is treated with a log averaging as

$$\rho^c_{typ}(\mathbf{K},\omega) = \exp\left(\frac{1}{N_c}\sum_{i=1}^{N_c}\langle\ln\rho^c_i(\omega,V_i)\rangle\right)\times \exp\left(\left\langle\ln\frac{\rho^c(\mathbf{K},\omega,V_i)}{\frac{1}{N_c}\sum_i\rho^c_i(\omega,V_i)}\right\rangle\right). \tag{15}$$

It is imperative to note that while there are different behaviors of the two methods around the re-entrance region (cf. Fig. 3), both procedures systematically converge to the same critical disorder strength e.g., $W_c^{N_c\geq 12} \approx 2.1 \pm 0.01$ for the box disorder distribution. However, the former (*linear-log* procedure) is generally more robust than the *log-log* method. The latter is characterized by slower convergence around the re-entrance region, requiring far larger cluster sizes before the convergence of the re-entrance region is achieved in comparison to the e.g., transfer matrix method (TMM) results. It may also not be adequate to study localization phenomena in realistic material applications, since it is not obviously clear how a geometrical averaging of the off-diagonal components of the spectral density, which are not positive definite, will be done. The comparison of the phase diagram obtained using the two procedures: *log-log* and *linear-log* formalisms is shown in Fig. 3. As is evident from the figure, the two new schemes converge to the same critical disorder strength but behave differently around the re-entrance region. While our original formulation (cluster typical medium theory (CTMT)) will eventually converge to a disorder strength far greater than W_c, a further remark is that the re-entrance trajectory of the mobility edge is totally missed as a consequence of self-averaging in the cluster.

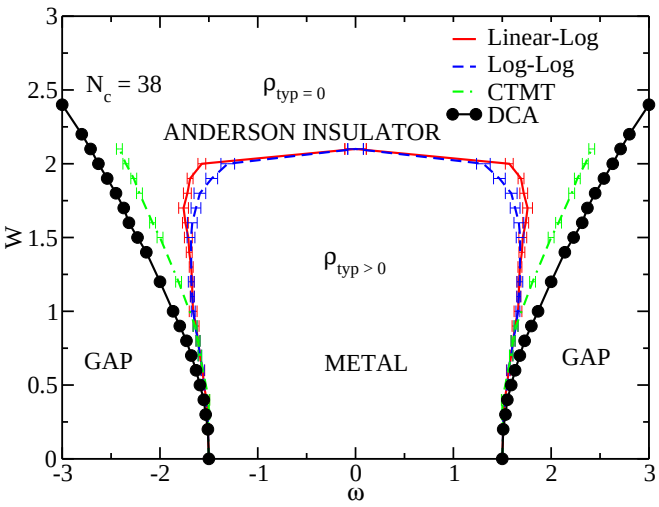

FIG. 3. (Color online). A comparison of the phase diagrams of the Anderson localization transition in 3D obtained from different cluster approximations with $N_c = 38$ using the CTMT and the TMDCA (linear-log and log-log) schemes. Observe that in the CTMT, as a consequence of self-averaging, the higher disorder behaviors which are captured in our TMDCA are totally missed and the critical disorder strength is also severely over-estimated.

We note that in both the *linear-log* and the *log-log* procedures, at small N_c, about 100 self-consistent iterations are required to achieve convergence, while, for relatively large N_c, far fewer iterations are required. The convergence criterion in both limits is achieved when the TDOS ($\omega = 0$) does not fluctuate anymore with iteration number within the error bars.

Finally, we note that many other definitions of the typical medium which avoid self-averaging are possible, in-

cluding the use of only the local part of Eq. 14, i.e.,

$$\rho^c_{typ}(K,\omega) = \exp\left(\frac{1}{N_c}\sum_{i=1}^{N_c}\langle \ln \rho^c_i(\omega, V_i)\rangle\right). \qquad (16)$$

However, this method was rejected since it does not meet most of the criteria discussed in the introduction. In this case, this formalism does not recover the DCA in the weak disorder limit.

3. *The Pole Procedure*

Close to criticality, the hybridization rate of the states at the top and bottom ($(0,0,0)$ and (π,π,π)) of the bands tends to zero leading to the development of poles in the cluster excluded Green function. Here, we present in detail how to deal with such poles that emerge on the real frequency axis as the critical disorder strength is approached.

When $\Im\Gamma_{typ}(\mathbf{K},\omega)$ becomes very small (i.e., $\Im\Gamma_{typ}(\mathbf{K},\omega) \to 0$), the imaginary part of the cluster-excluded Green function, $\mathcal{G}(\mathbf{K},\omega)$, becomes a series of delta functions. To see this, we note that

$$\begin{aligned}\mathcal{G}(\mathbf{K},\omega) &= (\omega - \Gamma_{typ}(\mathbf{K},\omega) - \overline{\epsilon}(\mathbf{K}) + \mu)^{-1} \qquad (17)\\ &= \mathcal{P}(\omega-\omega')^{-1} - i\pi\delta(\omega-\omega'),\end{aligned}$$

where $\omega' = \overline{\epsilon}(\mathbf{K}) - \mu + \Re\Gamma_{typ}(\mathbf{K},\omega)$ and "$\mathcal{P}$" denotes the principle value. Evidently from Eq. 17, the poles cannot be represented in the conventional way as a list of frequencies on the computer with a finite frequency resolution $d\omega$. Such difficulty can be avoided by replacing $\mathcal{G}(\mathbf{K},\omega)$ for each of the $\mathbf{K}-$cells where $\Im\Gamma_{typ}(\mathbf{K},\omega)$ is vanishing with

$$\mathcal{G}(\mathbf{K},\omega) = \begin{cases} -i\pi/d\omega & : \quad \omega = \omega' \\ \frac{1}{\omega-\omega'} & : \quad \omega \neq \omega'. \end{cases} \qquad (18)$$

We refer to this formulation as the explicit "*pole-procedure*". With this procedure, the singularity in $\mathcal{G}(\mathbf{K},\omega)$ can be properly captured. An added difficulty is that for a given N_c, as the W_c is approached, $\Im\Gamma_{typ}(\mathbf{K},\omega)$ for individual cells goes to zero at different rates. Hence, we have to determine which of these cells need to be treated with the explicit "pole-procedure". We choose the criterion that for any cell, if $(-1/\pi)\times\Im\Gamma_{typ}(\mathbf{K},\omega') < a\times d\omega'$, then, we apply the pole procedure to such cells. Here, $a \gtrsim 1$ is a parameter which measures the minimum number of pixels needed to represent a pole approaching the real frequency axis. Our numerical experience shows that such a criterion works nicely while spurious results are obtained otherwise.

A. Box Disorder Distribution

To demonstrate that the typical and not the average DOS can serve as a proper order parameter for the Anderson localization transition, we start the discussion of our results by comparing the algebraically averaged DOS (ADOS) calculated using DCA and the TDOS obtained from a single site TMT ($N_c = 1$) and finite clusters TMDCA ($N_c = 64$ and 125) at various disorder strengths W for the box disorder distribution (Eq. 2a). As shown in Fig. 4, the ADOS remains finite while the TDOS for both TMT and TMDCA continually gets suppressed as the critical disorder strength is approached. Moreover, one observes a crucial difference between the single site TMT ($N_c = 1$) and TMDCA finite clusters of $N_c = 64$ and 125. In the former, the mobility edge (for extended states TDOS is finite) defined by the boundary of the TDOS (indicated by arrows) always gets narrower with increasing disorder strength W, while in the latter, as a function of disorder strength, the mobility edge first expands and then decreases, hence giving rise to the re-entrance behavior, which is completely missing in the single-site TMT. Observe also the quick convergence with the clusters size at $\omega = 0$ for the finite clusters $N_c = 64$ and 125. The implications of this will be discussed fur-

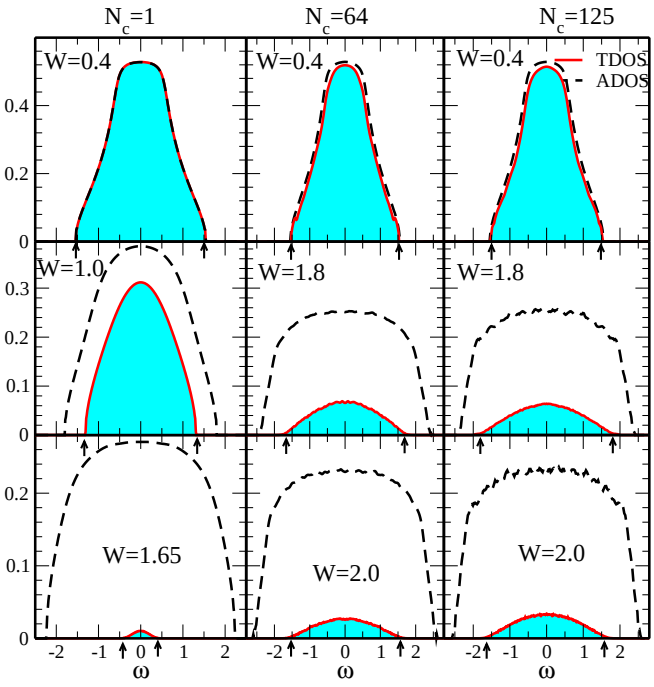

FIG. 4. (Color online). The evolution of the ADOS and TDOS at various disorder strengths W for the single-site TMT and the TMDCA with cluster size $N_c = 64$ and 125. At low disorder, where all the states are metallic, the shape of TDOS is the same as that of the ADOS. As W increases, in the case of single-site TMT, the TDOS gets suppressed and the mobility edge moves towards $\omega = 0$ monotonically. In the TMDCA, the TDOS is also suppressed, but the mobility edge first moves to higher energy,and only with a further increase of $W > 1.8$, it starts moving towards the band center, indicating that the TMDCA can successfully capture the re-entrance behavior. Arrows indicate the position of the mobility edge, which separates the extended electronic states from the localized ones and the colored region indicates the TDOS.

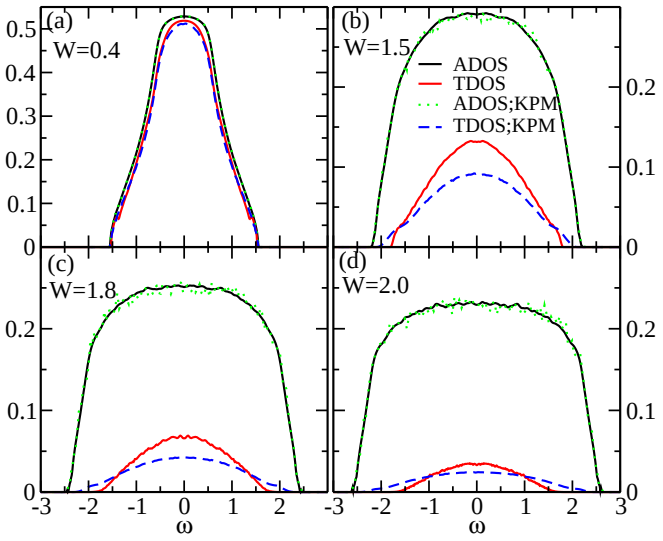

FIG. 5. (Color online). Comparison of the average (typical) density of states calculated with the DCA (TMDCA) and the kernel polynomial method (KPM) for the box disorder distribution at various strengths for the cluster size N_c=64. The kernel polynomial method used 4096 moments on a 48^3 cubic lattice, and 1000 independent realizations generated with 32 sites randomly sampled from each realization.

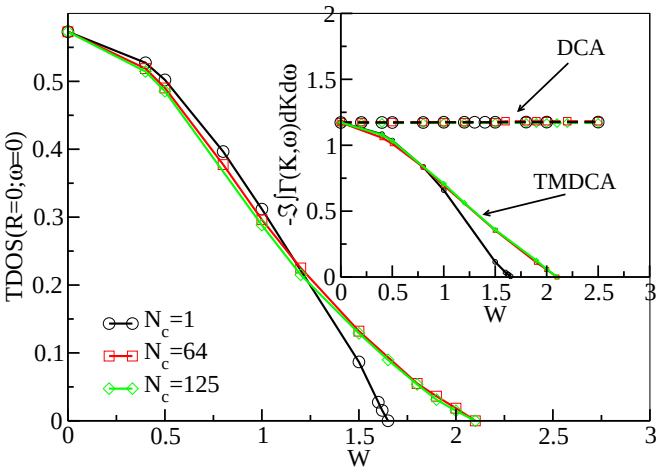

FIG. 6. (Color online). The TDOS($\omega = 0$) vs. disorder strength W at different cluster sizes $N_c = 1, 64$, and 125 for the uniform (box) disorder distribution. The TDOS($R = 0, \omega = 0$) vanishes at the critical disorder strength W_c. At $N_c = 1$, $W_c^{N_c=1} \approx 1.65$. As the cluster size increases, W_c systematically increases with $W_c^{N_c \gg 12} \approx 2.10 \pm 0.10$, showing a quick convergence with the cluster size. The inset shows the integrated hybridization function ($-\Im \int \Gamma(\mathbf{K}, \omega) d\mathbf{K} d\omega$) as a function of disorder strength W. Observe that $-\Im \int \Gamma(\mathbf{K}, \omega) d\mathbf{K} d\omega$ vanishes at the same disorder strength as the TDOS. The dashed lines are the $-\Im \int \Gamma(\mathbf{K}, \omega) d\mathbf{K} d\omega$ from the DCA. Observe that it is a constant regardless of the disorder strength and cluster size. This shows that the DCA, even though it incorporates spatial correlations, does not describe the Anderson localization transition. Moreover, near the critical region the TDOS($R = 0, \omega = 0$) data can be fitted to a power-law, with TDOS($R = 0, \omega = 0$) $= a_0 |W - W_c^{fit}|^\beta$. The obtained critical exponent for large enough clusters $\beta \approx 1.62 \pm 0.10$ is in good agreement with exact results. Note, the $-\Im \int \Gamma(\mathbf{K}, \omega) d\mathbf{K} d\omega$ data for $N_c = 64$ and 125 has been normalized with that of $N_c = 1$.

ther below and explored with respect to what happens to the trajectories of the mobility edge as the size of the cluster increases.

To benchmark our TMDCA formalism with another numerical technique, we utilize the kernel polynomial method.[8,9] We show in Fig. 5 a plot of the TDOS (ADOS) ($N_c = 64$) calculated using the TMDCA (DCA) as compared to the TDOS (ADOS) obtained using the kernel polynomial method (KPM). As it is evident from the plots, even though there is a qualitative agreement between the two methods, there are subtle deviations especially in the TDOS. This deviation can be attributed to finite lattice effects and the effective broadening due to the finite order expansion used in the KPM. Overall, the agreement is a manifestation of the ability of our TMDCA formalism[1] to accurately characterize the Anderson localization transition in systems with a uniform disorder distribution even with relatively small system sizes, as compared to the large lattice systems that need to be simulated in the kernel polynomial method for accurate results to be obtained.

Next, we consider the evolution of the critical disorder strength W_c with the cluster size. Figure 6 shows the local TDOS($\omega = 0$) at the band center as a function of disorder strength W for several cluster sizes: $N_c = 1, 64$, and 125. The critical disorder strength W_c is defined by the vanishing of the TDOS($\omega = 0$). The inset is the imaginary part of the integrated hybridization function which shares the same property as the TDOS since both vanish at the same disorder strength, while the DCA result remains finite, independent of the disorder strength, indicating no tendency towards localization with increasing disorder. Our results show that as N_c increases, the critical disorder strength W_c in the TMDCA systematically increases until it converges to the exact value $W_c \approx 2.10$[10,44–46,50–52,60] at cluster size $N_c \geq 12$. The cluster $N_c = 12$ is the first cluster with a complete nearest-neighbor shell based on Betts cluster classification.[61] From this cluster onward, W_c converges to ≈ 2.10, but the trajectory of the mobility edge in the re-entrance regime continues to change until it also converges to the exact results at larger N_c. This effect is due to the systematic incorporation of coherent backscattering as the cluster size increases and will be elaborated in more detail later.

To extract the order parameter critical exponent (β), we fit our data in Fig. 6 for the largest system size considered here ($N_c = 125$) using the power law: TDOS($\omega = 0$) $= a_0 |W - W_c^{fit}|^\beta$. Following the procedure as explained in Subsection III E, we obtain $\beta \sim 1.62 \pm 0.10$ with a corresponding critical disorder strength from the

fit $W_c^{fit} \sim 2.23 \pm 0.10$. The fit overestimates the critical disorder strength, as compared to the computed one, due to the difficulty in determining the scaling regime, as discussed below. This also causes the error bars to be larger than obtained from other methods. Nevertheless, the critical parameters from the fit are in good agreement with the recently reported value of $\beta \approx 1.67$.[46] It is also in general agreement with the values listed in Table III.

Apart from the typical density of states, the localization transition in the gapless single-particle excitations of the Anderson insulator can be studied using the return probability of an electron to a site.[58] The probability of quantum diffusion (or the return probability) describes the probability of a quantum particle (or a wave) to go from site l to l' in a time t. After disorder averaging, the return probability has basically three key contributions: a) the probability of going from site l to l' without any scattering, b) the probability of going from site l to l' by an incoherent sequence of multiple scattering (known as diffusion) and c) the probability to go from site l to l' via a coherent (or enhanced) multiple scattering processes (e.g., the *cooperon*).

In the DCA or TMDCA, it is more convenient to measure the probability of an electron remaining on a

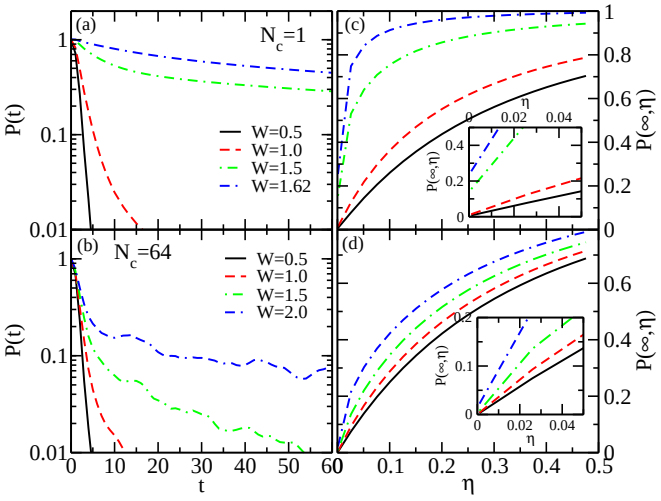

FIG. 7. (Color online). Right panels: The probability that an electron remains localized at all times $P(\infty,\eta)$ for the Anderson model for $N_c = 1$ and 64 at varying disorder strengths. We used the fact that $P(t\to\infty,\eta) = \lim_{\eta\to 0} \frac{-2i\eta}{N_c} \sum_l \int_{-\infty}^{\infty} d\omega d\omega' \left\langle \frac{\bar{A}(l,\omega)\bar{A}(l,\omega)}{\omega-\omega'-2i\eta} \right\rangle$, where $\bar{A}(l,\omega) = -1/\pi \Im \bar{G}(l,l,\omega)$ is the local coarse-grained (but not disorder averaged) spectra function. As $\eta \to 0$, $P(\infty,\eta)$ extrapolates to zero for small disorder strength indicating metallic behavior but does not extrapolate to zero anymore as the disorder strength is systematically increased towards the critical disorder strength leading to the transition (see the inset where this is manifestly illustrated). Left panels: The probability of an electron on a site thereby remaining trapped at finite time t for $N_c = 1$ and 64 for the same parameter as $P(\infty,\eta)$ on a semi-log plot.

given site l for all time $P(t\to\infty,\eta) = \lim_{t\to\infty} \left\langle |G(l,l,t)|^2 \right\rangle = \lim_{\eta\to 0} \frac{\eta}{\pi} \int_{-\infty}^{\infty} d\epsilon \left\langle |G(l,l,\epsilon+i\eta)|^2 \right\rangle$.[28] This will depend on the localization length, but if a significant fraction of the eigenstates of the disordered thermodynamic spectrum are localized states, $P(\infty,\eta)$ is expected to be nonzero.[28,53,58,59] Since the cluster is formed by coarse-graining the real lattice problem in **K**-space, there is a one-to-one correspondence between local quantities on the cluster and real space.[28] In Fig. 7 right panel, we show the $P(\infty,\eta)$ for the cluster sizes $N_c = 1$ and 64 for various disorder strengths. As it is evident from the plot, for relatively small disorder strength $W \sim 0.5$, $P(\infty,\eta)$ extrapolates to zero and becomes nonzero as the localization transition is approached. Just like the $P(\infty,\eta)$, the finite time probability that an electron on a site l remains after some time t denoted as: $P(t) = \left\langle |G(l,l,t)|^2 \right\rangle$ is a vital parameter for detecting the localization of electrons. As shown in Fig. 7 for $N_c = 1$ and 64 clusters, $P(\infty,\eta)$ and $P(t)$ contains the same information of the excitation spectra. In Fig. 7 left panel, we show the $P(t)$ for the same parameters as $P(\infty,\eta)$. Hence, a characteristic finite long time $P(t)$ denotes localized eigenstates. Again, systematic transition from a metallic regime (for small disorder) to an insulating regime (for a disorder strengths close to the critical value of the Anderson localization transition in $N_c = 1$ and 64 size clusters, respectively) is observed. Unlike in the DCA, the localization transition manifests clearly in the $P(\infty,\eta)$ and $P(t)$ calculated in the TMDCA since, even though the density of states (ADOS) calculated within the TMDCA is finite as in the DCA (the ADOS is a conserving quantity), the hybridization rate at the same energy depends highly on the strength of the disorder (cf. inset of Fig. 6). In fact, it vanishes continuously with the disorder strength and goes to zero at the same point where the typical density of states vanishes. Hence, since the hybridization rate between the cluster and the host vanishes continuously as the critical disorder strength is approached, the TMDCA method is able to capture the localization transition even when the ADOS calculated with the TMDCA is finite.

The probability distribution function (PDF) is another natural quantity to characterize the 3D Anderson localization transition due to the fact that the "typical" value of a "random" variable corresponds to the most probable value of the PDF.[33,50] A proper description of electron localization in disordered systems requires consideration of the distribution functions for the quantities of interest[2], so we calculate the PDF of the cluster-momentum-resolved DOS $\rho(K,\omega=\bar{\epsilon}_K)$ (at different momenta cells K and energy $\omega = \bar{\epsilon}_K$) sampled over a large number of disorder configurations.

In Figure 8, we show the evolution of the PDF$[\rho(K,\omega=\bar{\epsilon}_K)]$ with W. As is evident from the plot, for a relatively small disorder, the cells show a Gaussian distribution which gradually becomes log-normal and highly skewed as the critical disorder strength is approached.

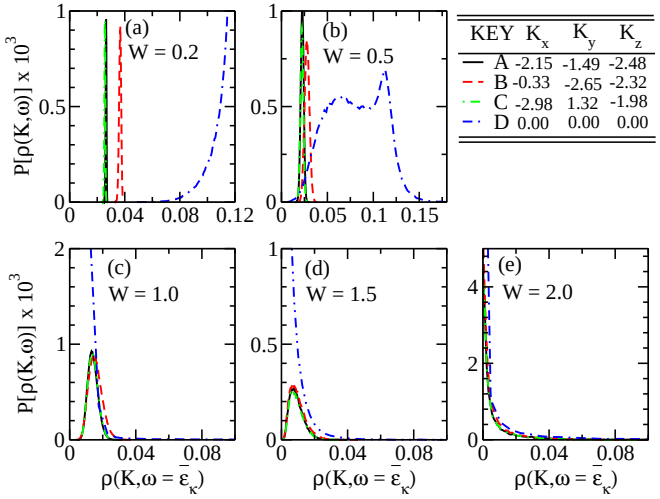

FIG. 8. (Color online). The evolution with disorder strength of the probability distribution of the density of states at different cluster cells for $N_c = 38$. Utilizing the irreducible wedge property and particle-hole symmetry, the original 38 cells are reduced to 4 cells. For small disorder strength, the cells show Gaussian distributions whereas close to the critical disorder strength $\simeq 2.0$, all the cells show log-normal distributions.

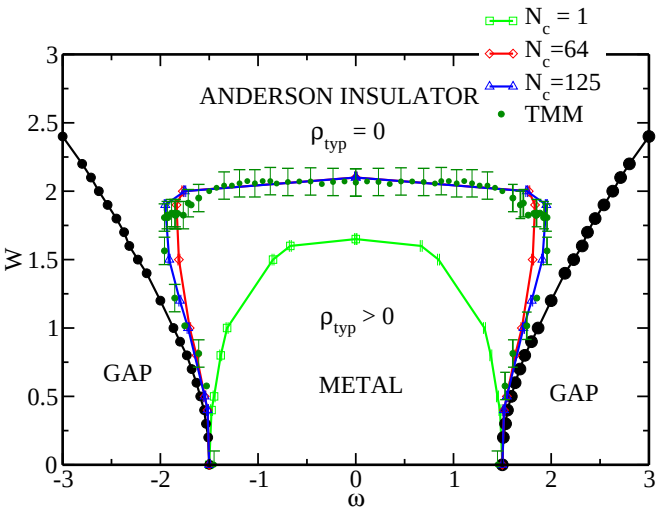

FIG. 9. (Color online). The phase diagram of the Anderson localization transition in 3D for the box disorder distribution obtained from TMDCA simulations. A systematic improvement of the trajectories of the mobility edge is achieved as the cluster size increases. At large enough N_c and within computation error, our results converge to those determined by the transfer matrix method (TMM). The TMM data is for system sizes of length $L = 1 \times 10^6$ (number of multiplications), the range of system widths used is $M = [2, 16]$ and reorthogonalization is done every 5 transfer matrix multiplications (see Appendix A for details). The error was determined in a point in the region of most discrepancy between the methods (upper bound of re-entrance) by a finite size scaling analysis (see Appendix A). The black line with filled circles denotes the Lifshitz boundaries (extracted from the ADOS calculated within the DCA).

The analysis of the spectra properties of the Anderson model[39,62] shows that for relatively small disorder strengths the states are still delocalized, and the amplitude of the wave functions associated with them is more or less the same on every site. The distribution of the local DOS with respect to disorder configurations is Gaussian with the most probable value coinciding with the arithmetic mean average value. However, for sufficiently large disorder strength or in the proximity of the band tails, the spectrum consists mainly of discrete eigenvalues, and the associated eigenfunctions are exponentially localized with substantial weight only on a few sites. The distribution is therefore extremely asymmetric (log-normal), with a most probable value much smaller than the arithmetic mean value. At this point, most of the weight is concentrated around zero. As is evident from Fig. 8, we indeed observe such behavior in our results.

We show in Fig. 9, the phase diagram of the Anderson localization transition in the disorder-frequency (W-ω) plane constructed from our TMDCA procedure for the box disorder distribution. Here, we show the mobility edge trajectories given by the frequencies where the TDOS vanishes at a given disorder strength W, and the band edge determined by the vanishing of the ADOS calculated within the DCA.

As is evident from Fig. 9, at $N_c = 64$ the W_c at $\omega = 0$ is the same as that for $N_c = 125$ but different from the $N_c = 1$ case. This shows that the W_c converges to ~ 2.10, while, the trajectory of the mobility edge continues to change with N_c. This may be understood from the different localization mechanisms for states at the band center and the edge.[51,63,64] Hence, for large enough clusters, we are able to converge to the exact result. In particular, as the cluster size N_c increases, the mobility edge trajectories are systematically reproduced, with the re-entrance behavior gradually captured with large cluster sizes. As we increase the cluster size the DOS systematically acquires states in the band tails, which are zero in the N_c=1 case (it is well known that single-site theories like CPA or TMT do not capture such states). According to Bulka *et al.*,[47,51] deep trapped states dictate the physics at large energies. Hence, by making $N_c > 1$ we systematically inject additional states that tend to push the localization edge outward. States at the band center become localized mainly due to coherent backscattering while those above and below the bare band edges are initially localized in deeply trapped states. They become delocalized with increasing W due to the increasing DOS at these energies and hence increasing quantum tunneling between the deeply trapped states. They finally become localized again with increasing disorder, which explains the re-entrant behavior. Since coherent backscattering requires a retracing of the electronic path, the effective length scales captured by the cluster are doubled, such that W_c converges very quickly at the band center. On the other hand, the quantum tunneling mechanism has

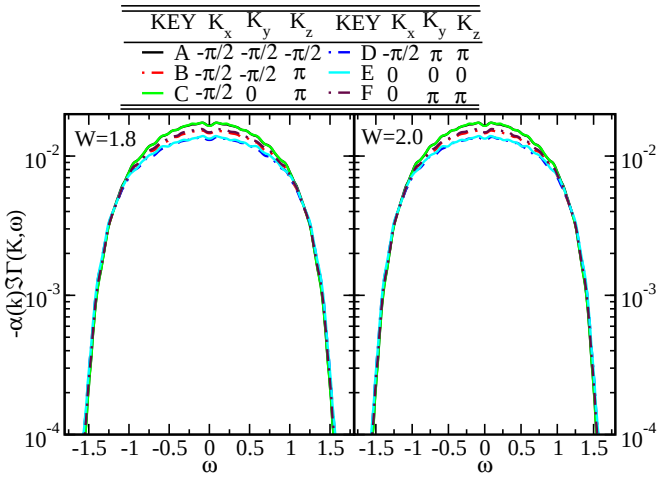

FIG. 10. (Color online). The scaling of the imaginary typical hybridization function ($-\Im\Gamma(\mathbf{K},\omega)$) for the 64 site cluster at disorder strengths of W = 1.8 and 2.0 on a semi-log scale. The labels A–F and their associated momenta $\mathbf{K}$ correspond to each of the six distinct cells obtained using the point-group and particle-hole symmetry ($\rho(\mathbf{K},\omega) = \rho(\mathbf{Q}-\mathbf{K},-\omega)$, with $\mathbf{Q} = (\pi,\pi,\pi)$) of the cluster). Observe that the mobility edges may be collapsed on top of each other by multiplying each of the hybridization functions with a constant such that $-\Im\Gamma(\mathbf{K},\omega) = -\alpha(\mathbf{K}) \times \Im\Gamma(\mathbf{K},\omega)$, where $\alpha(\mathbf{K})$ is a scaling constant, in agreement with Mott's idea of energy selective Anderson localization transition.

no path doubling and requires multiple deeply trapped states in the cluster and, therefore, converges more slowly with N_c.

Figure 10 is the scaling of the imaginary part of the typical hybridization function ($-\Im\Gamma(\mathbf{K},\omega)$) for $N_c = 64$ at $W = 1.8$ and 2.0, scaled by the factor $\alpha(\mathbf{K})$, so that the tails overlap. Even though different $\mathbf{K}$-cells go to zero at different rates, they each share the same unique mobility edge. Since the local disorder potential induces elastic scattering of a state at any momenta into any other with the same energy, there will be mixing of the localized and the extended states at the same energy. As a result, the localized and extended states cannot coexist at the same energy. Then the mobility edge can only exist at the point where all the states in each cell on the cluster are localized. As shown in Fig. 10, the collapse of the tails for all $\mathbf{K}$ such that $-\Im\Gamma(\mathbf{K},\omega) = -\alpha(\mathbf{K})\Im\Gamma(\mathbf{K},\omega)$, where $\alpha(\mathbf{K})$ is a scaling constant, validates Mott's idea of energy selective Anderson localization.[65,66]

B. Alloy Model

The application of the disordered tight-binding Hamiltonian (1) to the alloy model represents one of the most studied physical systems. This stems from the fact that the two potentials energies W_a and W_b depict the potential landscape of e.g., a binary alloy $A_{c_a}B_{1-c_a}$, with each of the sites occupied either by atom "A" or "B" with concentrations c_a and $c_b = 1 - c_a$, respectively.

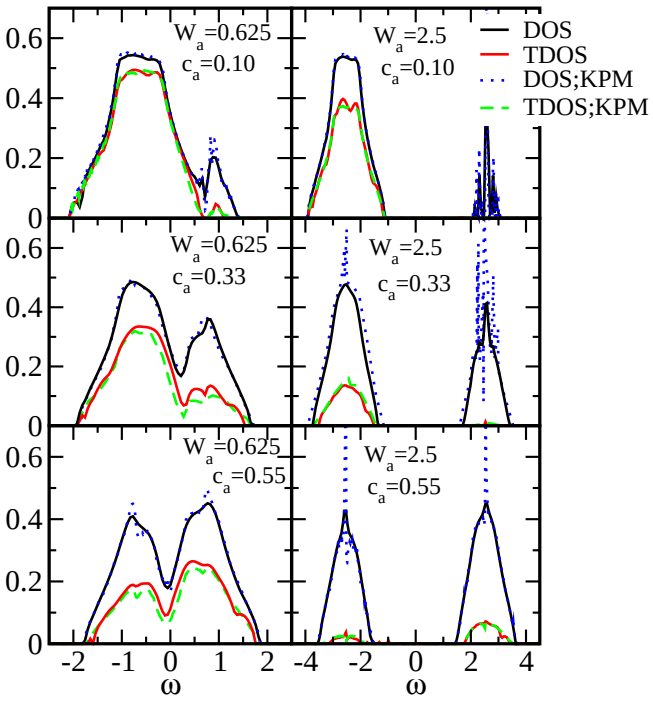

FIG. 11. (Color online). Comparison of the average (typical) density of states calculated with the DCA (TMDCA) and the kernel polynomial method (KPM) for the binary alloy system ($W_b = -W_a$) at various values of the local potential W_a and concentrations c_a for the cluster size N_c=125. The kernel polynomial method uses 2048 moments on a 48^3 cubic lattice, and 200 independent realizations generated with 32 sites randomly sampled for each realization.

To explore the applicability of our method for the study of binary alloys, we start the discussion of this section by showing in Fig. 11 the calculated typical (average) density of states from the TMDCA (DCA) procedure as compared to the TDOS (ADOS) calculated within the KPM[8,9,12–14] for various concentrations and disorder strengths. The importance of the TDOS is evident since for all the disorder strengths and concentrations, the ADOS remains finite around the two energies W_a and W_b, while the TDOS at a fixed concentration vanishes continuously with the strength of the disorder with smaller values in the sub-band with the lowest concentration. Fixing the strength of the disorder and varying the concentration, the sub-bands with the smallest concentration have fewer states. We note that there are subtle differences between the results for $N_c = 64$ (finite cluster) and single site $N_c = 1$ (CPA) (not shown) due to the incorporation of spatial correlations in the finite cluster which are missing in the local CPA. In fact, the TMT underestimates the extended region and misses small but important non-local features in the spectra.[67]

To further benchmark our results for the binary alloy model, let focus on the comparison of the average (typical) DOS calculated with the DCA and TMDCA

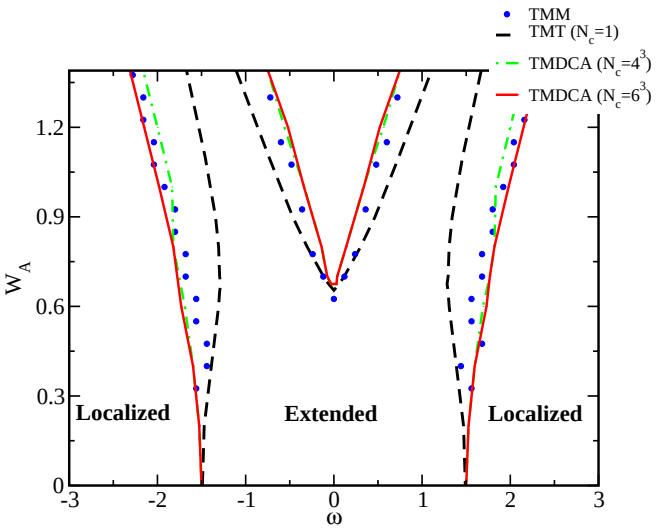

FIG. 12. (Color online). Disorder-energy (W_a-ω) phase diagram of the Anderson localization transition in 3D for the binary alloy system $A_{c_a}B_{1-c_a}$ for $c_a = 0.5$. Observe the systematic improvement of the trajectories of the phase diagram for the clusters ($N_c = 64$ and 216) in basic agreement with the numerical results from TMM. The system widths used for TMM are M=[6,12] and the length is scaled with the width as $L = M \times 10^4$. See Appendix A for details.

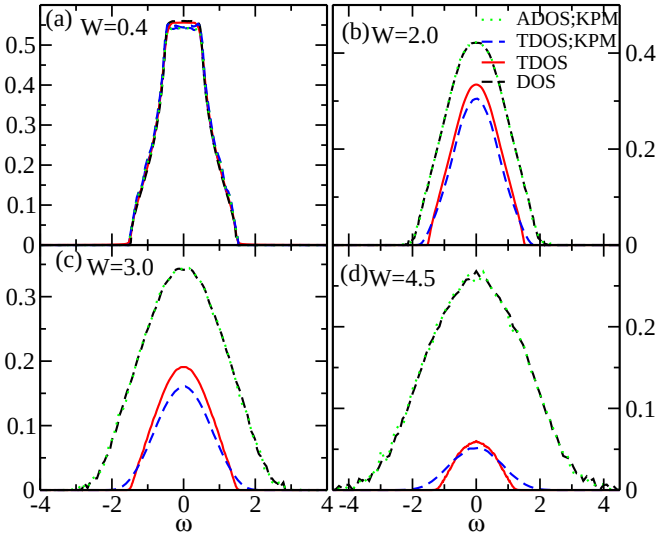

FIG. 13. (Color online). Comparison of the average (typical) density of states calculated with the DCA (TMDCA) and the kernel polynomial method (KPM) for the Gaussian disorder distribution at various values of the disorder strength for cluster size N_c=64. The kernel polynomial method uses 4096 moments on a 48^3 cubic lattice, and 1000 independent realizations generated with 32 sites randomly sampled from each realization.

($N_c = 64$) with the KPM data. As can be seen in Fig. 11, the TMDCA and DCA results reproduced those from the KPM, showing that our formalism offers a systematic way of studying the Anderson localization transition in binary alloy systems. Such a remarkable agreement is an indication of a successful benchmarking of the TMDCA method.[1]

We extract the mobility edges shown in Fig. 12 by finding the energy where the TDOS vanishes at a given value of the disorder potential. As can be seen in Fig. 12, the local $N_c = 1$ boundaries are narrower than those obtained for the finite cluster indicating that the TMT strongly underestimates the extended state regime. The comparison of the mobility edge boundaries for the TMDCA with those obtained from the TMM calculations show quite good agreement. This again is a confirmation of a successful benchmarking of the TMDCA for treating the binary alloy model. At the center of the band and for $c_a = 0.5$, we obtain a critical disorder strength W_c of $\approx$ 0.7 for the TMDCA in good agreement with the TMM (cf. Fig. 12).

C. Gaussian Disorder Distribution

The Gaussian (or normal) (Eq. 2b) is a unique distribution which other disorder distributions are built on and has many physical applications including the study of molecular-doped polymers.[68,69]

To further explore the versatility of our method, we apply it to study systems with the disorder defined by the Gaussian distribution function (Eq. 2b). Again, we use the typical density of states (TDOS) as the order parameter and the transition to the Anderson insulator is obtained at the disorder strength where the TDOS vanishes. The typical and average density of states obtained from the TMDCA and DCA, respectively, and those obtained from the kernel polynomial method are shown in Fig. 13 for various values of the disorder strength. As can be seen, the TDOS at all frequencies systematically goes to zero as the disorder strength increases while the ADOS remains finite. Again, our TMDCA formalism reproduces accurately the results from the kernel polynomial method. We note some subtle differences between the TDOS calculated from the TMDCA and the KPM while there are no noticeable differences in the average density of states from the DCA and KPM. This may be due to the finite broadening utilized in the KPM, which contributes additional tails to the already exponential tails of the TDOS. We remark that aside from the small initial broadening value (~ -0.01) used in the initialization of the TMDCA at the very first iteration, no broadening parameter is utilized for later iterations.

We show in Fig. 14, the evolution of the typical density of states TDOS($\omega = 0$) at the band center as a function of disorder strength for the local TMT ($N_c = 1$) and the TMDCA ($N_c = 64$ and 125). Our results indicate that the critical disorder strength (defined as the W where the TDOS vanishes) systematically increases as the cluster size is increased converging to $W_c \sim 5.30$ as soon as the size of the cluster $N_c \geq 12$. This is in good agreement with the numerically exact values of

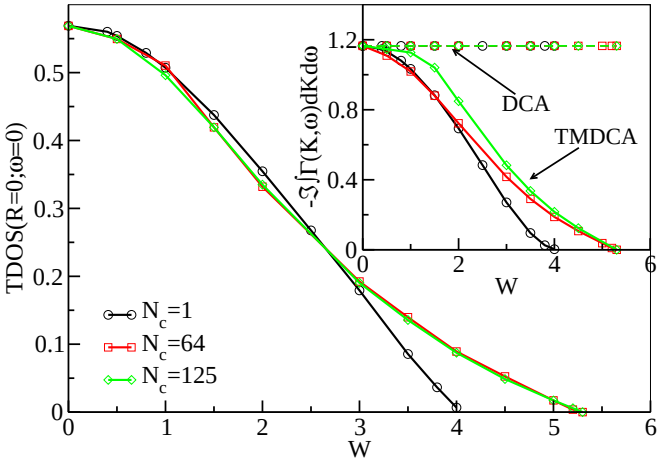

FIG. 14. (Color online). The TDOS($\omega = 0$) vs. disorder strength W at different cluster sizes $N_c = 1, 64$, and 125 for the Gaussian disorder distribution. The TDOS($\omega = 0$) vanishes at the critical disorder strength W_c. At $N_c = 1$, the critical disorder strength $W_c^{N_c=1} \approx 4.0$. As the cluster size increases, the critical strength systematically increases with $W_c^{N_c \gg 12} \approx 5.30 \pm 0.10$, showing a quick convergence with the cluster size. The inset shows the integrated hybridization function $(-\Im \int \Gamma(\mathbf{K}, \omega) d\mathbf{K} d\omega)$ as a function of disorder strength W. Observe that $-\Im \int \Gamma(\mathbf{K}, \omega) d\mathbf{K} d\omega$ vanishes at the same disorder strength as the TDOS. The dashed lines are the $-\Im \int \Gamma(\mathbf{K}, \omega) d\mathbf{K} d\omega$ from the DCA. Observe that it is a constant regardless of the disorder strength. This shows that the DCA, even though it incorporates spatial correlations does not describe the Anderson localization transition. Moreover, near the critical region the TDOS($\omega = 0$) data can be fitted to the power-law TDOS($\omega = 0$) $= a_0 |W - W_c^{fit}|^\beta$. The obtained critical exponent for large enough clusters $\beta \approx 1.57 \pm 0.10$ is in good agreement with the numerically exact results.[46] Note, the $-\Im \int \Gamma(\mathbf{K}, \omega) d\mathbf{K} d\omega$ data for $N_c = 64$ and 125 has been normalized with that of $N_c = 1$.

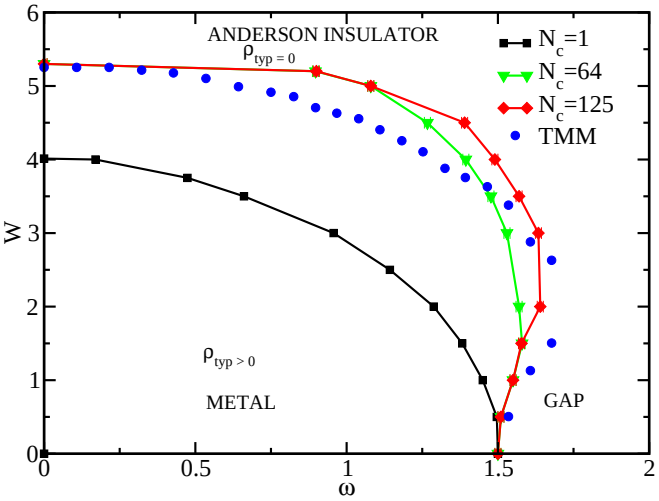

FIG. 15. (Color online). The phase diagram of the Anderson transition in 3D for the Gaussian disorder distribution obtained from TMDCA simulations. A systematic improvement of the trajectories of the mobility edge is achieved as the cluster size increases. At large enough N_c, our results converge to those determined by the TMM which are calculated for widths $M = [2, 16]$ and for a system length (number of transfer matrix multiplications) $L = 1 \times 10^6$, where the matrix products are reorthogonalized every 5 transfer matrix multiplications (see Appendix A). The deviation between the TMDCA and TMM results is consistent with the behavior observed for the box and Lorentzian disorders and can be attributed to the fact that a finite grid in energy is used for the TMDCA which tends to cause the typical density of states to be larger, hence slightly overemphasizing the metallic behavior and as such, the mobility edge is slightly larger when compared to TMM in certain frequency ranges near the band edge. The effect is most pronounced here due to the small density of states near the band edge. In addition, near the re-entrance regime, the TMM also has difficulties due to an increase in finite size effects (see Appendix A).

5.225 ± 0.125[47–49] and 5.32.[44] Fitting our data for the largest system size considered here ($N_c = 125$) using the power law: TDOS($\omega = 0$) $= a_0 |W - W_c^{fit}|^\beta$ and following the procedure as explained in Subsection III E, we obtain the order parameter critical exponent $\beta \sim 1.57 \pm 0.10$ with a corresponding critical disorder strength from the fit of $W_c^{fit} \sim 5.53 \pm 0.10$. This value of β is in good agreement with the value we obtained for the uniform disorder distribution (cf. Table II) and in good agreement with the recently reported value of $\beta \approx 1.67$.[46] It is also in general agreement with the values listed in Table III. The good agreement between the β we obtained from the uniform and Gaussian disorder distribution is a manifestation of the universal nature of the Anderson localization transition.[49,70]

To explore the trajectories of the mobility edge for the Gaussian disorder distribution, we show in Fig. 15 the phase diagram in the energy-disorder plane for various cluster sizes as compared to the TMM result.[47] For any given disorder strength W, the mobility edge is defined by the frequency where the TDOS vanishes. Unlike the critical disorder strength which converges quickly with the cluster size $N_c \geq 12$, the trajectory of the mobility edge continues to change with N_c converging to almost the numerically exact results for $N_c = 125$. The physical reasons for the quick convergence of W_c and the progressive change of the mobility edge with the cluster size is the same as those described above for the box disorder distribution (cf. Section III A). As can be seen, the single site TMT underestimates the extended region just as in the previously presented disorder distributions. There are, however, some subtle differences between our data and the TMM results around the re-entrance regime. The cause of this difference will be discussed in Section III F.

D. Lorentzian Disorder Distribution

We next apply our TMDCA formalism to study systems with the Lorentzian (or Cauchy) disorder distribution (cf. Eq. 2c). We show in Fig. 16 how the band

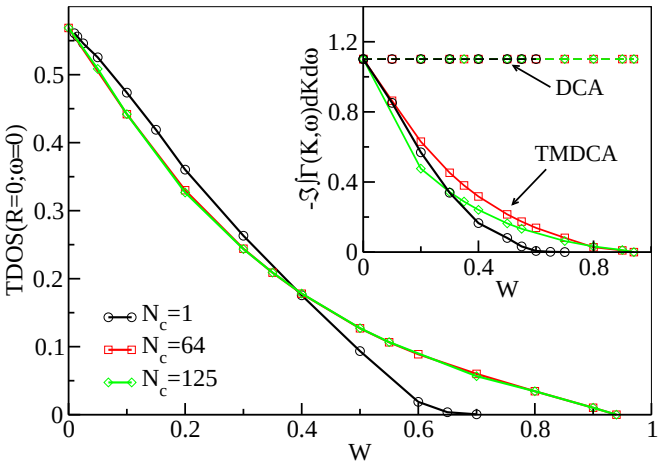

FIG. 16. (Color online). The TDOS($\omega = 0$) vs. disorder strength W at cluster sizes $N_c = 1$, 64, and 125 for the Lorentzian disorder distribution. The TDOS($\omega = 0$) vanishes at the critical disorder strength W_c. At $N_c = 1$, the critical disorder strength $W_c^{N_c=1} \approx 0.6$. As the cluster size increases, the critical strength systematically increases until $W_c^{N_c \gg 12} \approx 0.94 \pm 0.10$, showing a quick convergence with the cluster size. The inset shows the integrated hybridization function $(-\Im \int \Gamma(\mathbf{K}, \omega) d\mathbf{K} d\omega)$ as a function of disorder strength W. Observe that $-\Im \int \Gamma(\mathbf{K}, \omega) d\mathbf{K} d\omega$ vanishes at the same disorder strength as the TDOS. The dashed lines are the $-\Im \int \Gamma(\mathbf{K}, \omega) d\mathbf{K} d\omega$ from the DCA. Observe that it is a constant regardless of the disorder strength in agreement with the observations we have for other disorder distributions. We can fit the TDOS($\omega = 0$) data near the critical region to the power-law, with TDOS($\omega = 0$) $= a_0 |W - W_c^{fit}|^{\beta}$. The obtained critical exponent for large enough clusters $\beta \approx 1.60 \pm 0.10$ is in good agreement with numerically exact results.[46] Note, the $-\Im \int \Gamma(\mathbf{K}, \omega) d\mathbf{K} d\omega$ data for $N_c = 64$ and 125 has been normalized with that of $N_c = 1$.

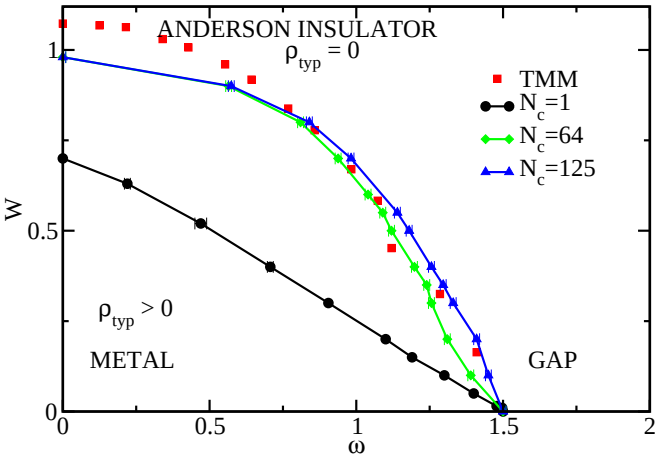

FIG. 17. (Color online). The phase diagram of the Anderson localization transition in 3D for the Lorentzian disorder distribution obtained from TMDCA simulations. The TMM data was computed for a system length of $L = 8 \times 10^5$ for system widths of $M = [2, 16]$ and re-orthogonalization is done every four multiplications (see Appendix A for details). The discrepancy between the TMDCA and TMM is due to the nature of the Lorentzian distribution as explained in Subsection III F.

center of the typical density of states (TDOS($\omega = 0$)) changes as the disorder strength is increased for the local TMT ($N_c = 1$) and the TMDCA ($N_c = 64$ and 125). As can be seen from Fig. 16, our results depict that the critical disorder strength systematically increases as the cluster size increases converging to $W_c \sim 0.94$ for $N_c \geq 12$ in good agreement with the numerically exact values of 0.95 ± 0.125[47–49] and 1.07,[44] respectively. Fitting our data for the largest system size considered here ($N_c = 125$) using the power law: TDOS($\omega = 0$) $= a_0 |W - W_c^{fit}|^{\beta}$ (see Subsection III E for the description of how the β is extracted), we can infer the order parameter critical exponent $\beta \sim 1.60 \pm 0.10$ with a corresponding critical disorder strength from the fit, $W_c^{fit} \sim 0.97 \pm 0.10$. The obtained β from our fit is in good agreement with the values listed in Table III and in good agreement with the recently reported value of $\beta \approx 1.67$.[46] This β value of the Lorentzian disorder distribution is also in good agreement with the values we obtained for the box and Gaussian disorder distributions, respectively. This further illustrates the universal nature of the Anderson localization transition.[49,70]

We conclude our study of the application of the typical medium dynamical cluster approximation to the Lorentzian disorder distribution by presenting in Fig. 17 the phase diagram in the energy-disorder plane. Unlike the box and Gaussian disorder distributions, our simulations show that the Lorentzian distribution does not have re-entrance of the mobility edge. The lack of re-entrance of the mobility edge in the Lorentzian disorder distribution may be attributed to the absence of finite variance in this form of distribution. For the single site CPA ($N_c = 1$), the critical parameters are woefully underestimated. However, we systematically converge to the numerically exact results as the size of the cluster is increased. As it is obvious from Fig. 17, for as small as $N_c = 64$, we converge almost to the exact TMM results.[51] We again see remarkably good agreement between our effective mean-field method for the Anderson localization transition and the numerically exact calculations.

E. Critical Parameters

The critical parameters, including the critical disorder strength W_c and the order parameter critical exponent β are summarized in Table II for different cluster sizes using the box disorder distribution as a case study. W_c^{cal} was determined as the W where the TDOS $(\omega = 0)$ vanishes. Observe that as N_c increases, W_c^{cal} systematically increases with $W_c^{cal} \approx 2.10 \pm 0.01$, showing a quick convergence with N_c.

The order parameter critical exponent β is obtained by fitting the power law: TDOS$(\omega = 0) = a_0 \times |W - W_c^{fit}|^{\beta}$

TABLE II. The calculated and fitted critical disorder strengths W_c^{cal} and W_c^{fit} and the order parameter critical exponent β obtained from our fit for the box disorder distribution. W_c^{cal} is defined by the vanishing of the TDOS ($\omega = 0$). β and W_c^{fit} are obtained by fitting the TDOS($\omega = 0$) data with a power law, TDOS($\omega = 0$) $= a_0|W - W_c^{fit}|^{\beta}$.

N_c	W_c^{cal}	W_c^{fit}	β
1	1.66±0.01	1.65±0.10	0.96±0.10
64	2.10±0.01	2.18±0.10	1.46±0.10
125	2.10±0.01	2.23±0.10	1.62±0.10

directly to our data and systematically searching for the best data point away from the transition where the fit still follows the actual data (scaling regime). This becomes imperative since away from the transition, the data is not expected to fit the form TDOS($\omega = 0$) $= a_0 \times |W - W_c^{fit}|^{\beta}$ and also close to the transition, there should be a crossover to a mean field form since the TMDCA treats the longest length scales in a mean field approximation. So, the fit may only be done between these limits. The ambiguity in the determination of the fitting region increases our error bars on the exponent, and causes W_c^{fit} to be overestimated. In addition, the strong fluctuation of the TDOS in the proximity of the critical point also increases our error bars. We show in Fig. 18 a comparison plot of the fit and our data for the 125 site cluster for the box, Lorentzian, and Gaussian disorder distributions, respectively. The fit of the power law to the scaling region of the data gives the value of the β in an unambiguous manner. The obtained values of β from the various cluster sizes, for instance, for the box disorder distribution are shown in Table II. One can see that our β systematically approaches the numerical experimental value[44,46,50] for large enough clusters (here, largest N_c simulated is 125) as listed in Table III for the box, Gaussian, and Lorentzian disorder distributions, respectively, and in comparison with other numerical values.

F. Difficulties in Extracting the Mobility Edge at Higher Disorder

As explained in the previous sections, the mobility edge is obtained by locating the frequencies where the typical density of states vanishes at a given disorder strength W. The band edge is determined by the vanishing of the average density of states calculated within the DCA. As it is obvious from the phase diagrams for the various disorder distributions (Figs. 9, 15, and 17, respectively), there are some discrepancies between the phase diagram obtained within the typical medium dynamical cluster approximation and the transfer matrix method. They can be attributed in part to the form of the disorder distribution. For example, the bare DOS for the Gaussian and Lorentzian disorder distributions are known to have exponential tails. The severity of the exponential nature of the tails associated with the various disorder distributions increases as box, Gaussian, and Lorentzian, in that order. At these higher disorder strengths (once a mobility edge develops), the TDOS naturally develops tails. We note that in our computations, apart from the initial small broadening value ~ -0.01 used in the initialization of the self-energy (needed only for the first iteration), no

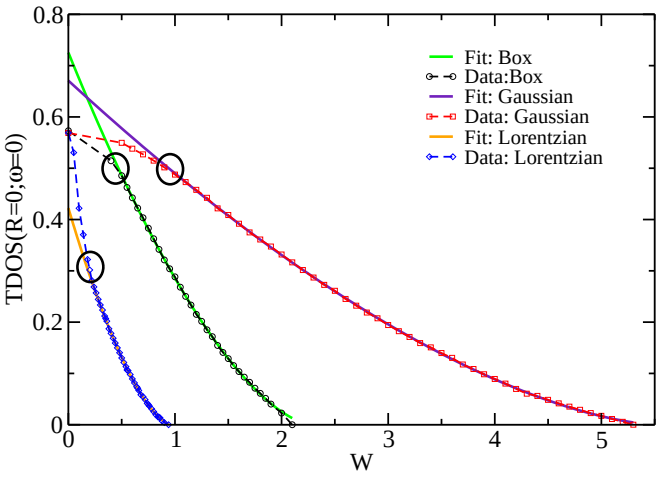

FIG. 18. (Color online). The band center of the typical density of states (TDOS($R = 0; \omega = 0$)) at various disorder strengths (W) for the 125 site cluster for the Box, Gaussian, and Lorentzian disorder distributions. The linear region of the data can be fit with a scaling ansatz: TDOS($\omega = 0$) $= a_0 \times |W - W_c^{fit}|^{\beta}$, with $\beta \sim 1.62$ for the Box disorder distribution, $\beta \sim 1.57$ for the Gaussian disorder distribution, and $\beta \sim 1.60$ for the Lorentzian disorder distribution in good agreement with the recently reported value of $\beta \approx 1.67$.[46,50] The circles in the plot depict the data point where the fit starts to deviate from the data.

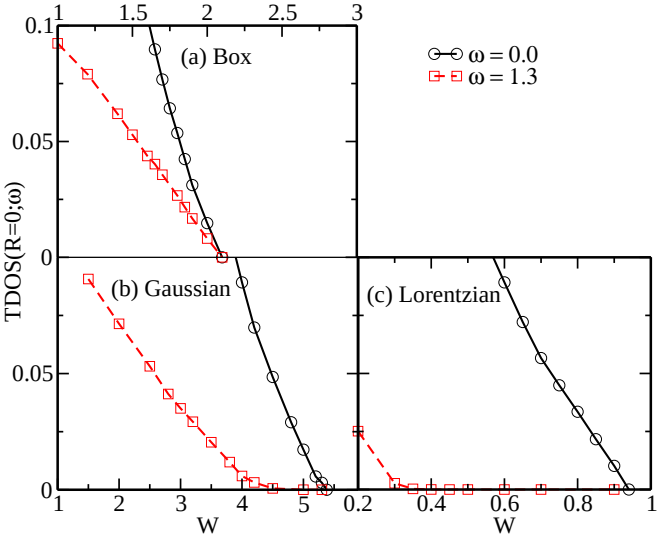

FIG. 19. (Color online). The plot of the typical density of states (TDOS) at $\omega = 0.0$ and $\omega = 1.3$ for various disorder strengths for the (a) Box, (b) Gaussian, and (c) Lorentzian disorder distributions.

TABLE III. Critical parameters of the Anderson localization for the various studied disorder distribution in 3D obtained using the TMDCA in comparison with the numerically exact results. We use $4t = 1$ as our energy unit. We note that the critical exponents (β and ν) are independent of disorder distribution (universal) as verified by the multifractal analysis,[49] the analytic results of Wegner,[70] and detailed finite size scaling.[15] Abbreviations used in the Table are: transfer matrix method (TMM), multifractal finite size scaling (MFSS), level statistics (LS), kicked rotor (KR), and experimental atomic waves (Exp-AW).

Author	Critical Disorder			Critical Exponent		Method
	Bo	Ga	Lo	ν	β	
Present study	2.10±0.10	5.30±0.10	0.94±0.10	–	1.57–1.62	TMDCA
Slevin *et al.*[a]	2.067	–	1.067	1.573–1.577	–	TMM
Slevin *et al.*[b]	2.068–2.073	5.32	1.066	1.58	–	TMM
Slevin *et al.*[c]	2.056±0.014	–	–	1.59–1.60	–	TMM
Rodriguez [d]	2.066–2.067	–	–	1.59	1.65–1.68	MFSS
Rodriguez [e]	2.066–2.071	–	–	1:58±0.03	–	MFSS
Markos[f]	2.063,2.067	–	–	1.47–1.55	–	MFSS
MacKinnon[g]	2.063 ±0.05	–	–	1.54±0.08	–	TMM
MacKinnon *et al.*[h]	2.063 ±0.063	–	–	1.2±0.3	–	TMM
Bulka *et al.*[i]	2.038–2.063	5.23±0.13	0.95±0.13	–	–	TMM
Milde *et al.*[j]	–	–	–	1.62±0:07	–	TMM
Shklovskii *et al.*[k]	2.0±0.063	–	–	1.50±0.15		LS
Zharekeshev *et al.*[l]	2.05	–	–	1.4±0.15	–	LS
Hofstetter [m]	2.719±0.012	–	–	1.35±0.15	–	LS
Lopez [n]	–	–	–	1.63±0.05	–	KR
Grussbach *et al.*[o]	2.02	5.23	–	1.32±0.02–1.37±0.02	1.32±0.02–1.37±0.02	MFSS [a]
Lemarié [p]	–	–	–	1.58±0.01–1.60±0.03	–	KR [b]
Lemarié [p]	–	–	–	1.40±0.30	–	Exp-AW [c]

The order parameter critical exponent β and the correlation length critical exponent ν can be transformed from one to the other using the hyperscaling relation of Ref. (46) $\beta = (\alpha_o - d)\nu$, where α_o is the Lipschitz-Hölder exponent which gives the maximum value of the multifractal spectrum. The most recent estimates as reported in Ref. (46) are $\alpha_o = 4.048$, $\nu = 1.59$ and $\beta = 1.67$.

[a] The authors obtain $\alpha_o = 4.0$ such that in the hyperscaling relation $\beta = (\alpha_o - d)\nu$, β equals ν.
[b] Authors of this paper show that their quasiperiodic kicked rotor belongs to the same (orthogonal) universality class as the 'random' Anderson model.
[c] Authors of this paper reported that experiments were done on the atomic kicked rotor by a sequence of kicks to the atomic cloud and measure its dynamics.
[a] Ref. 15.
[b] Ref. 44, 45.
[c] Ref. 71.
[d] Ref. 46.
[e] Ref. 50.
[f] Ref. 72.
[g] Ref. 73.
[h] Ref. 10.
[i] Ref. 47, 51.
[j] Ref. 74.
[k] Ref. 75.
[l] Ref. 76.
[m] Ref. 77.
[n] Ref. 78.
[o] Ref. 49.
[p] Ref. 79, 80.

broadening factor is utilized. As such, these tails that emerge as the disorder strength is increased towards W_c are physical tails since the top and bottom of the bands will localize first. To demonstrate this, we show in Fig. 19 a plot of the TDOS at $\omega = 0.0$ and $\omega = 1.3$ for the box, Gaussian, and Lorentzian disorder distributions, respectively. Note the $\omega = 1.3$ frequency is arbitrary but chosen such that it is close to the re-entrance region of the mobility edge. As can be seen from the plots, for the box disorder distribution, even though there are small tails, the TDOS at $\omega = 0.0$ and $\omega = 1.3$ behave alike and differ only in magnitude. There are no obvious long tails in either frequency ($\omega = 0.0$ and 1.3) that may mask the detection of the position of the mobility edge energies.

However, for the Gaussian and Lorentzian disorder distributions, there are exponentially long tails especially at $\omega = 1.3$ that make pinpointing the exact position of the mobility edge energies highly non-trivial. This should further be understood from the fact that unlike the box disorder distribution, the Lorentzian disorder distribution naturally has tails that decay very slowly at infinity, as $|x|^{-2}$, such that aside the zeroth moment (the area under the curve), all other higher moments do not even exists.

We note that this difficulty is generic not only to the TMDCA but also for any method where the extraction of the trajectories of the mobility edge is based on the TDOS. A notable example is in the kernel polynomial method, which even shows more severe discrepancies (not shown).

This deviation between the TMDCA and TMM at higher disorder strengths can also be attributed to the fact that the TMDCA, just like the KPM utilizes a finite frequency grid (which biases more towards the metallic regime) in contrast to the TMM which calculates the transmission of electrons at fixed energies. Even so, we note that the TMM also has its own shortcomings away from the band center due to the strong fluctuations in the Kramer-MacKinnon scaling parameter Λ (see Appendix A for its definition) as can be seen from the phase diagrams for the various disorder strengths around the re-entrance regime.

IV. CONCLUSIONS

Here, we present a detailed study of the Anderson localization transition using the recently developed typical medium dynamical cluster approximation (TMDCA) for the box, Gaussian, Lorentzian, and binary alloy disorder distributions in three dimensions. For each distribution we find the TMDCA to be a successful, causal, numerically efficient, self-consistent and rapidly convergent method for the study of localization in disordered electron systems.

With our formalism, we demonstrate that the typical DOS vanishes for localized states and is finite for extended ones. Employing the typical DOS as an order parameter for Anderson localization, we have constructed the disorder-energy phase diagram, extracted the order parameter critical exponent (β) for each disorder distribution, and benchmarked them in good agreement with other numerically exact methods. Within our precision, we find that β for the Anderson localization transition is a universal parameter independent of disorder distribution in agreement with the multifractal analysis.[49] For distributions with a finite variance (box and Gaussian), we demonstrate that there are extended states outside the unperturbed band.

We further show using the DCA (which includes spatial correlations) and a variant of the typical medium theory (which includes spatial correlations but suffers from self-averaging), the importance of the effective medium to properly characterize the Anderson localization transition. We also demonstrate the inability of the single site CPA and the TMT methods to accurately capture the localization and disorder effects in both the average and the typical DOS. We note that the single site TMT, while being able to qualitatively capture the localization transition, strongly underestimates the extended regions and fails to capture the critical parameters including the mobility edge trajectories and the exponents. In contrast, the TMDCA captures nicely the trajectories of the mobility edge with great improvement in the critical order parameter exponent. Most significantly, the TMDCA results are in a quantitative agreement with exact numerical results.

The TMDCA formalism is computationally inexpensive and straightforward to implement since it requires only the computer time needed to invert small clusters (e.g., $N_c = 1$–125), average over the disorder configurations, and iterate to convergence. Since only a small cluster is needed to get reliable data, material specific details may be incorporated. Once combined with electronic structure calculations[81] and more sophisticated many-body techniques for electron interactions, it will open a new avenue for studying localization phenomenon in real materials as well as the competition between disorder and electron correlations. To demonstrate the high efficiency of the TMDCA, as only small clusters are needed to get a converged result in good agreement with the TMM data, we compare the relative CPU time needed for the largest system size simulated in the TMDCA and the TMM. For the largest cluster size used in the TMDCA calculations, which is $N_c = 216$, the compute time is $\sim$4 hours (running on a single processor). While for the TMM, which is perfectly parallel in both disorder and frequency, each point in the phase diagram can require significant computational effort. For example, the system sizes in Fig. 9 used $\sim$20 hours on 64 processors per frequency. Since a separate TMM calculation is needed for each frequency, achieving the energy resolution of a typical TMDCA calculation (for a certain number of frequency grid points) would require the product of the number of processors used to parallelize over disorder times the number of grid points. As a calculation of a real material would require even larger system sizes than used here in the TMM, the TMDCA would prove much more computational efficient for the purpose of studying real materials.

Acknowledgments– We thank Shuxiang Yang and Vladimir Dobrosavljević for useful discussions. We also thank Janee Jarrell for a careful reading of the manuscript. This work is supported by NSF DMR-1237565 and NSF EPSCoR Cooperative Agreement EPS-1003897 with additional support from the Louisiana Board of Regents, and the DOE Computational Materials and Chemical Sciences Network (CMCSN) SC0007091. Supercomputer support was provided by the Louisiana Optical Network Initiative(LONI), and HPC@LSU computing resources.

Appendix A: Details of the Transfer Matrix Method

We benchmark our TMDCA results for the mobility edge with the transfer matrix method (TMM),[4,10–14] which is an established numerical method for determining the mobility edge by computing the localization length in disordered quantum systems. TMM is based on an iterative formulation of the Schrödinger equation where the wave function amplitude is computed at each site in a quasi-one-dimensional "bar" of length L and width M by successive multiplications of the transfer matrix that describes the transmission between each "slice" of size M^{d-1}. Thus, the Lyapunov exponent that measures the exponential decay of the wavefunction is explicitly computed, yielding the localization length. The system length L is the total number of transfer matrix multiplications. The numerical instability of the repeated multiplications is avoided by periodically orthogonalizing the transfer matrix product with a Lapack QR decomposition after a finite number of iterations.[15] The transfer matrix method finite size effects are larger for weak disorder where the states decay slowly with distance and so have large values of the localization length, which results in more pronounced fluctuations in the data. Notice that the CPA and the DCA (same as the TMDCA) do not suffer such finite size effects for small disorder and are, in fact, exact in this limit.

The mobility edge is obtained by calculating the dimensionless Kramer-MacKinnon scaling parameter Λ_M, which is the localization length divided by M.[12] Λ_M scales as a constant for $M \to \infty$ at the transition.[13] Precise values of the critical disorder may be measured directly from the crossing plots of Λ_M vs. W. A finite size scaling is performed by expanding Λ_M near the critical point using

$$\Lambda_M = f(M/\xi) \approx \Lambda_c + a_1|W-W_c|M^{1/\nu} + a_2|W-W_c|^2 M^{2/\nu} + \cdots \tag{A1}$$

and the data is fit using a least squares procedure.[36] The data used in Fig. 9 was a third order polynomial in $|W - W_c|M^{1/\nu}$. The critical disorder strength W_c from the finite size scaling is averaged over many generated data sets via a bootstrap procedure.[15] Any errors quoted in the TMM data are from the difference in the measured critical disorder from the finite size scaling analysis[12] and the critical disorder measured directly from the crossing plots of Λ_M vs. W.

Appendix B: Details of the Kernel Polynomial Method

To further benchmark our results, we utilize the kernel polynomial method to calculate the local DOS.[6–9] In the kernel polynomial method analysis, instead of diagonalizing the Hamiltonian directly, the local DOS is expanded in term of an infinite series of Chebyshev polynomials. In practice, the truncated series leads to Gibbs oscillations. The kernel polynomial method damps these oscillations by a modification of the expansion coefficients. We use the Jackson kernel following previous studies on the Anderson model.[8]

* Electronic address: cekuma1@lsu.edu
† Electronic address: jarrellphysics@gmail.com

[1] C. E. Ekuma, H. Terletska, K.-M. Tam, Z.-Y. Meng, J. Moreno, and M. Jarrell, Phys. Rev. B **89**, 081107 (2014).
[2] P. W. Anderson, Phys. Rev. **109**, 1492–1505 (1958).
[3] E. Abrahams, P. W. Anderson, D. C. Licciardello, and T. V. Ramakrishnan, Phys. Rev. Lett. **42**, 673 (1979).
[4] B. Kramer and A. MacKinnon, Rep. Prog. Phys. **56**(12), 1469 (1993).
[5] F. Evers and A. D. Mirlin, Rev. Mod. Phys. **80**, 1355 (2008).
[6] R. N. Silver and H. Röder, Inter. J. Mod. Phys. C **05**(04), 735 (1994).
[7] R. N. Silver and H. Röder, Phys. Rev. E **56**, 4822 (1997).
[8] A. Weiße, G. Wellein, A. Alvermann, and H. Fehske, Rev. Mod. Phys. **78**, 275 (2006).
[9] G. Schubert and H. Fehske, *in:* B. K. Chakrabarti, K. K. Bardhan, and A. K. Sen (eds.) *Quantum and Semi-classical Percolation and Breakdown in Disordered Solids*, *Lecture Notes in Physics*, vol. 762, 1–28 (Springer Berlin Heidelberg, 2009).
[10] A. MacKinnon and B. Kramer, Phys. Rev. Lett. **47**, 1546–1549 (1981).
[11] B. Kramer and M. Schreiber, *in:* K. H. Hoffmann and M. Schreiber (eds.) *in Computational Physics*, 166–188 (Springer, Berlin, 1996).
[12] A. MacKinnon and B. Kramer, Z. Phys. B **53**, 1–13 (1983).
[13] B. Kramer, A. MacKinnon, T. Ohtsuki, and K. Slevin, Int. J. Mod. Phys. B **24**, 1841 (2010).
[14] P. Markoš, Acta Physica Slovaca **56**, 561 (2006).
[15] K. Slevin and T. Ohtsuki, New J. Phys. **16**, 015012 (2014).
[16] E. Domany and S. Sarker, Phys. Rev. B **20**, 4726 (1979).
[17] L. Root and J. L. Skinner, Phys. Rev. B **33**, 7738 (1986).
[18] A. Singh and W. L. McMillan, J. Phys. C **18**(10), 2097 (1985).
[19] A. Abou-Chacra, D. J. Thouless, and P. W. Anderson, J. Phys. C **6**, 1734 (1973).
[20] D. Vollhardt and P. Wölfle, *in Electronic Phase Transitions* (Elsevier Science, Amsterdam, 1992).
[21] G. Schubert, J. Schleede, K. Byczuk, H. Fehske, and D. Vollhardt, Phys. Rev. B **81**, 155106 (2010).
[22] D. Vollhardt and P. Wölfle, *Self-Consistent Theory of Anderson Localization* (W. Hanke, Yu. V. Kopaev (eds.), Electronic Phase Transitions, Elsevier, 1992).
[23] P. Soven, Phys. Rev. **156**, 809 (1967).
[24] B. Velický, S. Kirkpatrick, and H. Ehrenreich, Phys. Rev. **175**, 747–766 (1968).

[25] V. Dobrosavljević, A. A. Pastor, and B. K. Nikolić, EPL **62**(1), 76 (2003).
[26] M. Jarrell, T. Maier, C. Huscroft, and S. Moukouri, Phys. Rev. B **64**, 195130 (2001).
[27] S. Kirkpatrick, B. Velický, and H. Ehrenreich, Phys. Rev. B **1**, 3250 (1970).
[28] M. Jarrell and H. R. Krishnamurthy, Phys. Rev. B **63**, 125102 (2001).
[29] M. H. Hettler, M. Mukherjee, M. Jarrell, and H. R. Krishnamurthy, Phys. Rev. B **61**, 12739 (2000).
[30] M. Tsukada, J. Phys. Soc. Jpn. **26**, 684 (1969).
[31] D. Thouless, Phys. Rep. **13**, 93 (1974).
[32] D. J. Thouless, J. Phys. C **3**, 1559 (1970).
[33] C. E. Ekuma, H. Terletska, Z. Y. Meng, J. Moreno, M. Jarrell, S. Mahmoudian, and V. Dobrosavljević, J. Phys.: Conden. Matt. **26**(27), 274209 (2014).
[34] R. J. Elliott, J. A. Krumhansl, and P. L. Leath, Rev. Mod. Phys. **46**, 465 (1974).
[35] T. Maier, M. Jarrell, T. Pruschke, and M. H. Hettler, Rev. Mod. Phys. **77** 1027 (2005).
[36] T. Nakayama and K. Yakubo, *Fractal Concepts in Condensed Matter Physics*, *Springer Series in Solid-State Sciences*, vol. 140 (Springer, 2003), ISBN 9783540050445.
[37] A. D. Mirlin and Y. V. Fyodorov, Phys. Rev. Lett. **72**, 526 (1994).
[38] A. Lagendijk, B. van Tiggelen, and D. S. Wiersma, Physics Today **62**, 24 (2009).
[39] M. Janssen, Phys. Rep. **295**, 1–91 (1998).
[40] J. Brndiar and P. Markoš, Phys. Rev. B **74**, 153103 (2006).
[41] E. Miranda and V. Dobrosavljevic, *Conductor Insulator Quantum Phase Transitions*, chap. Dynamical mean-field theories of correlation and disorder, 161–235 (Oxford University Press, 2012).
[42] M. Janssen, Int. J. Mod. Phys. B **8**, 943 (1994).
[43] E. Crow and K. Shimizu (eds.) *Log-Normal Distribution–Theory and Applications* (Marcel Dekker, NY, 1988).
[44] K. Slevin and T. Ohtsuki, Phys. Rev. Lett. **82**, 382 (1999).
[45] K. Slevin and T. Ohtsuki, Phys. Rev. B **63**, 045108 (2001).
[46] A. Rodriguez, L. J. Vasquez, K. Slevin, and R. A. Römer, Phys. Rev. B **84**, 134209 (2011).
[47] B. Bulka, M. Schreibe, and B. Kramer, Z. Phys. B **66**, 21 (1987).
[48] B. Kramer and M. Schreiber, *in: Fluctuations and Stochastic Phenomena in Condensed Matter*, *Lecture Notes in Physics*, L. Garrido (ed.), vol. 268, 351 (Springer Berlin Heidelberg, 1987), ISBN 978-3-540-17206-2.
[49] H. Grussbach and M. Schreiber, Phys. Rev. B **51**, 663 (1995).
[50] A. Rodriguez, L. J. Vasquez, K. Slevin, and R. A. Römer, Phys. Rev. Lett. **105**, 046403 (2010).
[51] B. Bulka, B. Kramer, and A. MacKinnon, Z. Phys. B **60**, 13 (1985).
[52] G. Schubert, A. Weibe, G. Wellin, and H. Fehske, *HPC in Sci. & Eng., Garching 2004* (Springer, 2005).
[53] A. Gonis, *Green functions for ordered and disordered systems* (North-Holland Amsterdam, 1992).
[54] E. Gross, E. Runge, and O. Heinonen, *Many-Particle Theory* (A. Hilger, Bristol, 1991), ISBN 9780750301558.
[55] A. Fetter and J. Walecka, *Quantum Theory of Many-particle Systems*, Dover Books on Physics (Dover Publishers Incorporated, 1971).
[56] D. D. Johnson, Phys. Rev. B **38**, 12807 (1988).
[57] P. R. C. Kent, M. Jarrell, T. A. Maier, and T. Pruschke, Phys. Rev. B **72**, 060411 (2005).
[58] D. J. Thouless, Phys. Rep. **17**, 93 (1974).
[59] E. Müller-Hartmann, Z. Phys. B **76**(2), 211 (1989).
[60] Y. Song, W. A. Atkinson, and R. Wortis, Phys. Rev. B **76**, 045105 (2007).
[61] D. D. Betts and G. E. Stewart, Can. J. Phys. **75**, 47 (1997).
[62] J. Fröhlich, F. Martinelli, E. Scoppola, and T. Spencer, Communications in Mathematical Physics **101**(1), 21 (1985).
[63] B. Kramer, I. Zharekeshev, and O. Halfpap, *in: Advances in Solid State Physics*, B. Kramer (ed.), vol. 39, 253 (Springer Berlin Heidelberg, 1999).
[64] B. Kramer and M. Schreiber, *in: Localization in Disordered Systems*, W. Weller and P. Ziesche (eds.), vol. 16, 96 (Teubner Texte zur Physik (BSB Teubner, Leipzig), 1988).
[65] N. F. Mott, *Metal-Insulator Transitions, 2nd ed.* (Taylor and Francis, London, 1990).
[66] N. Mott, J. Phys C **20**(21), 3075 (1987).
[67] H. Terletska, C. E. Ekuma, C. Moore, K.-M. Tam, J. Moreno, and M. Jarrell, Phys. Rev. B **90**, 094208 (2014).
[68] J. M. Sin and Z. G. Soos, Philosophical Magazine **83**(7), 901 (2003).
[69] K. Sienicki, Macromolecules **24**(1), 270 (1991).
[70] F. Wegner, Nucl. Phys. B **316**, 663 (1989).
[71] K. Slevin and T. Ohtsuki, Phys. Rev. Lett. **78**, 4083 (1997).
[72] P. Markos, J. Phys. A **33**(42), L393 (2000).
[73] A. MacKinnon, Journal of Physics: Condensed Matter **6**(13), 2511 (1994).
[74] F. Milde, R. Römer, M. Schreiber, and V. Uski, Eur. Phys. J. B **15**(4), 685–690, ISSN 1434-6028 (2000).
[75] B. I. Shklovskii, B. Shapiro, B. R. Sears, P. Lambrianides, and H. B. Shore, Phys. Rev. B **47**, 11487 (1993).
[76] I. K. Zharekeshev and B. Kramer, Phys. Rev. Lett. **79**, 717 (1997).
[77] E. Hofstetter, Phys. Rev. B **57**, 12763 (1998).
[78] M. Lopez, J.-F. Clément, P. Szriftgiser, J. C. Garreau, and D. Delande, Phys. Rev. Lett. **108**, 095701 (2012).
[79] G. Lemarié, J. Chabé, P. Szriftgiser, J. C. Garreau, B. Grémaud, and D. Delande, Phys. Rev. A **80**, 043626 (2009).
[80] G. Lemarié, B. Grémaud, and D. Delande, EPL (Europhysics Letters) **87**(3), 37007 (2009).
[81] D. D. Johnson, D. M. Nicholson, F. J. Pinski, B. L. Györffy, and G. M. Stocks, Phys. Rev. B **41**, 9701 (1990).